Framework of Graphene Oxide (FOG) Synthesis and its Application as Supercapacitor

A dissertation submitted to the Department of Chemistry, Quaid-i-Azam University, Islamabad, in partial fulfillment of requirements for the degree of

Master of Philosophy

in

Inorganic/Analytical Chemistry

by

Hafiz Muhammad Zohaib
Reg. No.02061611007
Department of Chemistry
Quaid-i-Azam University
Islamabad
2016-18


بسم الله الرحمن الرحيم

Dedicated to

To my mother

And

My father

Who always has confidence in me and offered me encouragement and support in all my endeavors

And

Supervisor

Prof. Dr. Illayas Sarwer

Acknowledgments

All praises for the **Almighty Allah**, Who guides us in darkness and helps us in difficulties, Who has bestowed man with intelligence, wisdom and knowledge, and all respects to **Holy Prophet Hazrat Muhammad** (Peace be upon him) who exhorted his followers to seek for knowledge from cradle to grave and who enable us to recognize our creator. Foremost, I would like to express my sincere gratitude to my advisor ***Prof. Dr. Illayas Sarwer***, for his continuous support during my MPhil study and research, for his patience, motivation, enthusiasm, and immense knowledge. His guidance helped me in all the time of research and writing of this thesis. I could not have imagined having a better advisor and mentor for my MPhil work. I am thankful to ***Prof. Dr. Muhammad Siddiq*** (Chairman chemistry Department) and ***Prof. Dr. Amin Badshah*** (Head of Inorganic/Analytical section). Thanks to my friends for their valuable help and encouragement during my research. Without their assistance none of this would have been possible. Last but certainly not least special thanks and deepest appreciations are extended to my beloved, learned and zealous Father; my success is really the fruit of his devoted prayers and encouragement

Hafiz Muhammad Zohaib

Abstract

Graphene oxide (GO) was synthesized by environmental friendly improved Hummers method. The para-xylylenediamine (1,4-XDA) and 2,6-diaminopyridine (2,6-DAP) modified frameworks of graphene oxide (FGO) were synthesized by a facile solution processing. Different samples were prepared varying the amount of 1,4-XDA and 2,6-DAP. Characterization of graphene oxide (GO) and framework of graphene oxide (FOG) was performed by different analytical techniques like UV-Vis Spectroscopy, FTIR, XRPD, SEM, TGA, BET etc. The synthesized FOG materials were employed as active working electrode materials in three electrode system for the study of their behaviour as supercapacitor. The electrochemical properties and the mechanism how these materials improved the electrochemical performance were investigated systematically. 1,4-XDA and 2,6-DAP molecules incorporated between the graphene sheets demonstrated a loose and crumpled microstructure. The maximum specific capacitance value was found for FOG-X-A i-e 360 Fg^{-1} and minimum for FOG-D-C i-e 29.37 Fg^{-1}. The results revealed the role of amine-based organic additives in graphene supercapacitor materials and verified the FOG-X-A as the electrode materials of supercapacitor with an excellent electrochemical performance.

List of Schemes

List of Abbreviations

GO	Graphene oxide
FOG	Frameworks of Graphene oxide
1, 4-XDA	para-Xylylenediamine
2, 6-DAP	2, 6-Diaminopyridine
CVD	Chemical vapor dispersion
XRD	X-ray diffraction
TGA	Thermal gravimetric analysis
SEM	Scanning electron microscopy
BET	Brunauer–Emmett–Teller
CV	Cyclic Voltammetry
EIS	Electrochemical Impedance spectroscopy

Table of Figures

List of Tables

Table of Contents

Chapter 1 Introduction

1.1 Brief History of Graphite

The name graphite carbon is derived from the Latin word “carbo” meaning charcoal. This element is distinctive and form well-known stable allotropes, as its electronic structure allows for sp, $sp^2$and sp^3 hybridized networks. Graphite an abundant natural mineral is the most common crystalline allotropic form of carbon and has been known ever since antiquity together with diamond. Graphite has a planar, layered structure consists of atomic layers of sp^2 hybridized carbon atoms stacked together via van der waals force. The carbon atoms in every layer are arranged in honey comb like lattice with 0.142 nm separation and d-spacing between planes is 0.34 nm. All atoms in plane are covalently bonded; merely three of the four bonding sites are satisfied, however, the fourth electron is allowed freely to move in the plane making graphite electrically conductive in the direction parallel to the plane. Though the vast delocalized electrons are available in between the layers, so at right angle to the plane it is non-conductive in nature [1].

1.2 Graphene

The individual layer of sp^2 hybridized carbon atoms firmly packed into a two-dimensional (2D) hexagonal honeycomb like crystal lattice is called graphene [2]. This name was first introduced by Stumpp, Setton and Boehm, in 1994 [3]. It acts as the basic building block for graphitic derivatives of all other dimensionalities, such as fullerenes (0D), carbon nanotubes (1D) and graphite (3D) [4]. Graphene is a semi-metal with zero bandgap due to slight overlap between the valence and the conduction bands (zero bandgap material). In the graphene layer each carbon atom form three sigma bonds by overlapping of sp^2 orbitals with neighboring carbon atoms whereas the band of filled π-orbital (valance band) and empty π^* orbitals (conduction band) is formed by the overlapping of the remaining p_z orbitals which are accountable for the high in-plane electrical and thermal conductivity.

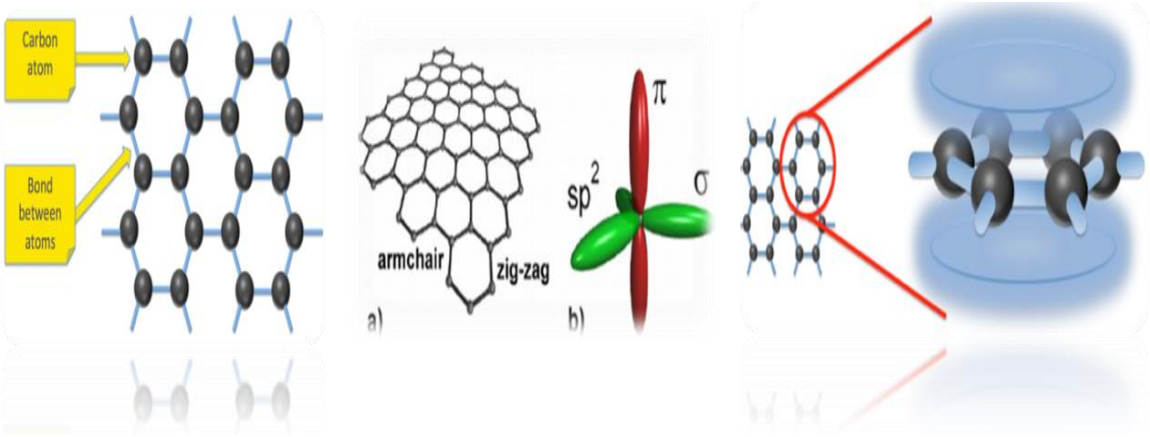

Figure 1.2 Graphene geometry

Graphene has the exceptional outstanding properties including high electron mobility i.e, upto 200,000 $cm^2V^{-1}s^{-1}$ [5], high mechanical strength i.e, Young's modulus ~1 T Pa [6], outstanding thermal conductivity i-e $5000Wm^{-1}K^{-1}$, 97.7% optical transparency [7] and large specific surface area approximately 2630 m^2g^{-1} hence, it has drawn marvelous attention from researchers. Graphene-based sheets have been used in high performance catalysis [8], nanocomposites [9], high performance energy storage devices [10], chemical and biological sensors [11], optoelectronics and electronics [12] etc.

1.3 Graphite Oxide and Graphene Oxide

Graphite oxide has a stacked or layered structure like graphite, but in graphite oxide graphitic carbon is well decorated by oxygenated functionalities, which not only make the graphite oxide hydrophilic in nature but also enhance its interlayer spacing. These oxidized graphite oxide layers can exfoliate in water or other solvents under ultrasonication. If the highly exfoliated sheets like graphene have one or few carbon atom layers, then these are named as graphene oxide (GO). GO has a mono atomic layered structure composed of carbon, oxygen and hydrogen molecules synthesized by the oxidation of inexpensive and abundantly existed graphite crystals. Due to its hydrophilic character it can disperse in water more easily than other solvents and convenient to process. Most importantly the graphene oxide can be reduced partially by the reduction of oxygenated groups to graphene sheets. The chemically derived GO have given many other names as functionalized graphene oxide, frame works of graphene, reduced graphene or chemically modified graphene.

i. Graphene oxide (GO) have two significant features: GO can be synthesized or produced with high yield via cost effective chemical route using cheap graphite as a raw material.

ii. As GO is hydrophilic in nature it can form highly stable aqueous colloids to aid the formation of macroscopic structures by inexpensive and simple solution process.

The graphene sheets comprise of trigonally bonded sp^2 hybridized carbon atoms and apart from micro-ripples it's completely flat. However, GO sheets partly compose of tetrahedral bonded sp^3 hybridized carbon atoms, which are slightly displaced below or above the graphene plane. Because of the existence of covalently bonded functional moieties and structural deformation, the sheets of graphene oxide are atomically rough. Several researchers have investigated and observed that the surface of graphene oxide has defective regions due to the presence of oxygen and the other areas are almost intact. According to a report honey comb like lattice structure remain preserved in GO as like graphene, however, slight displacement of carbon atoms due to attached functional groups but the size of the unit cell remains the same as that of graphene. Hence forth GO can be defined as irregular oxidized oxygen containing regions along with non-oxidized areas having sp^2 hybridized carbon atoms.

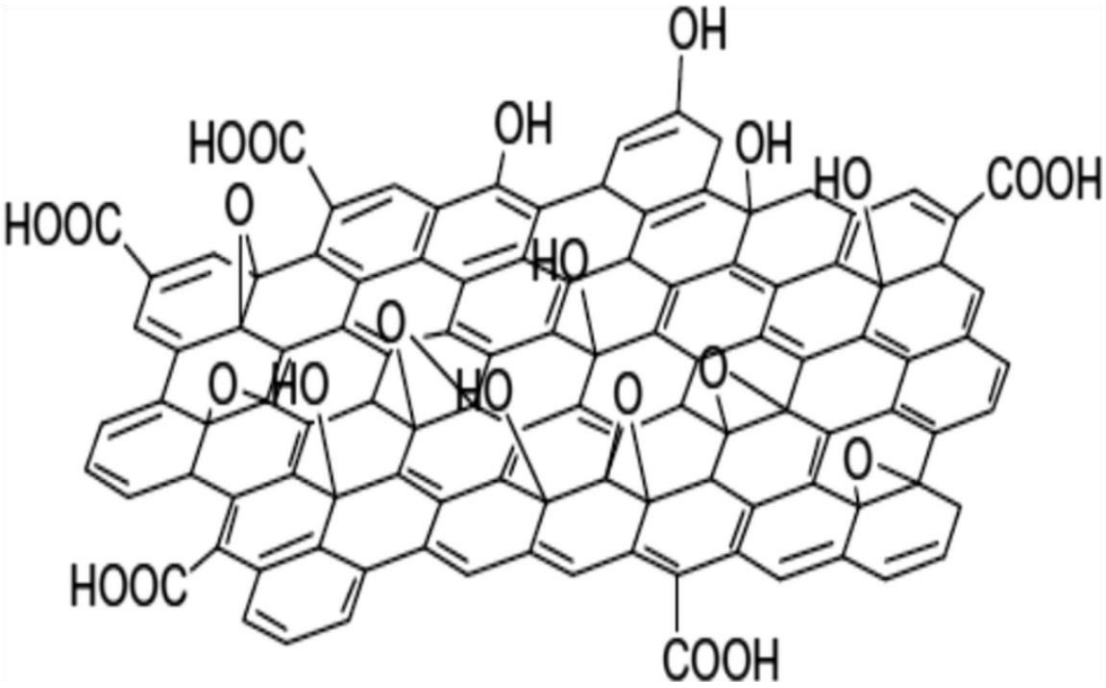

Figure 1.3 Framework of GO

1.4 Graphite Functionalization

As the interplanar distance (d-spacing) between the stacked layers of the graphite valued to be 0.34 nm and is not adequate to host inorganic and organic ions/molecules or other species. However, in order to enhance the graphite interlayers spacing from 0.335nm to higher values numerous intercalation approaches have been applied, depending on the size of the guest species. Ever since the intercalation of graphite with potassium, a series of chemical species have been tried to make what we called graphite intercalation compounds (GICs). These compounds could be formed by the insertion of intercalated species between the graphene layers via polar or ionic associations without altering the graphene structure. GICs can be synthesized not only with alkali metals (like sodium, potassium, lithium etc.) but also with anionic species like bisulfate, nitrate, or halogens.

In some cases, the inserted molecules may interact with covalent bonding through chemical grafting reactions within the graphite interlayer spacing; this results in the structural changes of the graphene planes as the hybridization changes from sp^2 to sp^3 of the reacting graphitic carbon atoms. A characteristic example of GICs is the reaction of graphite with strong acids and oxidizing agents that generates oxygen functional groups not only on the surfaces but also at the edges of the graphene layers results into the formation of graphite oxide.

First, in 1840 Schafheutl [13] and after 19 years in 1859 Brodie [14] were the pioneers in the formation of graphite oxide. The earlier fabricated graphite oxide with a mixture of nitric and sulfuric acid, while the later treated fuming nitric acid and potassium chlorate with raw graphite material. Staudenmaier [15] modified the Brodie method where oxidation of the graphite was done by the addition of concentrated H_2SO_4 and HNO_3 with potassium chlorate. After a century Hummers and Offeman [16] in 1958, reported that by immersing graphite in a mixture of $NaNO_3$, H_2SO_4, and KMnO4 oxidation occurs by the reaction of intercalated anions with carbon atoms of the graphitic layers resulted into the loss of the aromatic character. The robust oxidative reaction of these species with graphite leads to the generation of anionic groups mostly carboxylates, hydroxylates and epoxy groups on the surface and edges of the graphitic layers. The out of plane covalent bonds (like C–O) enhance the spacing between the graphene layers from 0.34 nm in graphite to around 0.68 nm [17] in graphite oxide. This newly developed polar or anionic character and enhanced inter spacing due to oxygen containing groups makes GO strongly hydrophilic in nature, which permits water molecules to penetrate within the graphene sheets thus forced the layers to further move

apart. Thus graphite oxide can more easily in water than any other solvent. During the formation of graphite oxide the hybridization of carbon atoms changed from sp^2 to sp^3 which results into the disruption of the delocalized π system and thus electrical conductivity deteriorates between 103 to 107 Ω cm according to the quantity of oxygen [1, 18].

1.5 Graphene Oxide Frame Works

To inhibit the agglomeration of the GO sheets and to enhance the performance of graphene-based semiconductors [19], numerous methods have been introduced [20, 21]. These methods modify graphene properties by introducing covalently or non-covalently dopants or fillers to GO sheets [22, 23]. For example, conducting polymers [24], carbon nanotubes [25, 26], heteroatoms [24] and transition metal oxides [27] were studied and adopted for graphene oxide (GO) surface modifications, which would inhibits the aggregation or restacking of graphene layers or sheets and they may server as the spacers or may add redox active functional species that would enhance the capacitance of GO. However, some disadvantages have been associated with non-covalent approaches, like the molecules may slip pass over each other, and they are unstable and difficult to control in contrast to the covalent approaches [28]. Therefore, for this purpose the covalent approaches are more promising way.

As reported previously, phenylenediamine as a good molecule for the graphene oxide functionalization and it is quite effective to enhance the performance of the SCs [29, 30]. It is well known that GO has large number of highly reactive functional groups on its surface, which allows the grafting of small organic molecules covalently on GO layers/sheets by different reactions [31]. The PPD (p-phenylenediamine) has two amine groups ($–NH_2$) on the benzene ring para-position that may react in certain conditions with the functional moieties present on the surface of GO layers, thus prevents the restacking or aggregation of the GO sheets by occupying the space between the graphene layers .Though, many researchers find out PPD as a good redox mediator and it accelerates the pseudocapacitance of SCs by rapid reversible faradaic reactions. Furthermore, PPD is also viewed as nitrogen doping precursor for the capacitance enhancement [32]. Here, in our thesis we report the 1,4-XDA and 2,6-DAP modified GO composite materials by using the solution process. 1,4-XDA and 2,6-DAP functionalized GO composite materials have been used as the electrodes materials of SCs, exhibiting excellent electrochemical performance.

1.6 Methods for the production of GO

It is always remain challenging to produce Graphene oxide and modified graphene oxide materials in massive quantity and of high quality by using inexpensive, cheap and environmentally friendly methods.

1.6.1 Mechanical Exfoliation

Mechanical exfoliation can be used for the production of the pristine graphene oxide but the drawback of this method is that its highly complicated and the small amount of product can be achieved which limits its large scale production.

1.6.2 Chemical Vapor Deposition

CVD technique can also be used for the synthesis of graphene films with one or few layer thickness. The drawback of this process is that it requires elevated temperature upto1000 $^{\circ}$C along with hydrogen as carrier gas and a flow of hydrocarbon precursor gas which limits or restricts its application range.

1.6.3 Epitaxial Growth

In this process pure graphene with excellent properties and perfect structure is synthesized. But it is not east to assemble the product in thin films due to its extremely small size. In addition to this, high energy is required during this process which restricts its application and use for large scale production

1.6.4 Chemical Methods

Chemical methods are one of the best method uses now days for the production of the pristine graphene and graphene modified materials. These methods include:

1.6.4.1 Brodie and Staudenmaier Methods

Graphene oxide (GO) was initially synthesized by Brodie in 1859 during his research work on graphite [33]. The raw graphite was oxidized by adding potassium chlorate ($KClO_3$) to the mixture of graphite and nitric acid (HNO_3). The resulting light yellow color graphene oxide

was obtained after repeatedly washing, filtration and drying and the product obtained is stable to further oxidation.

Staudenmaier modified the Brodie's work by mixing the graphite and nitric acid (HNO_3) mixture more acidic and followed by the gradual addition of $KClO_3$ to this mixture. These variations and modifications simplified the process and improved the GO quality. However, the drawback of this method is to take long time for $KClO_3$ addition and as a by-product toxic gas chlorine dioxide is released.

The mixture of $KClO_3$ and HNO_3 was used earlier for the fabrication of nanotubes [34], fullerenes [35]. However, the oxidation results into the production of many oxygen containing functional moieties such as lactose, ketones, carboxyl's and also discharge toxic gases dinitrogen tetraoxide (N_2O_4) and nitrogen dioxide (NO_2). That's why this method still needs modification.

1.6.4.2 Modified and Improved Hammers Methods

Hummer and its coworkers developed a method for the synthesis of GO termed as Hummers method [16]. In this process the water free mixture of $NaNO_3$, conc. H_2SO_4 and $KMnO_4$ was maintained for two hours below 45°C. The product obtained had a high degree oxidation as compared to the previously reported Staudenmaier method, however, in Hummer's method it was found that the product has GO sheets along with some un-oxidized graphite. For the excellent complete oxidation of graphite pretreated hummers method was introduced by Kovtyukhova. He first added raw graphite material to the mixture of potassium persulfate ($K_2S_2O_8$), conc. H_2SO_4, and phosphorous pentaoxide (P_2O_5), this mixture was maintained at 80°C for several hours[36]. This preoxidized product was then washed, filtered and dried in air. In 2010, Marcano *et.al* reported modified hummers method [37]. In place of $NaNO_3$ they added phosphoric acid (H_3PO_4) and also increase the amount of potassium permanganate. This minimize the discharge of hazardous gases due to the removal of sodium nitrate thus prohibits the emission of N_2O_4, NO_2 and ClO_2. In improved hummers method [38] graphite is first mixed with conc. H_2SO_4 to form GIC and then followed by the gradual addition of $KMnO_4$ then deionized water is added followed by the addition of H_2O_2. The product is then washed with 30% HCl and deionized water and dried to obtain the GO (Figure 1.6.4.2).

In brief summary, the improved hummers method have the potential for the mass production of GO without the discharge of any sludge or toxic gases.

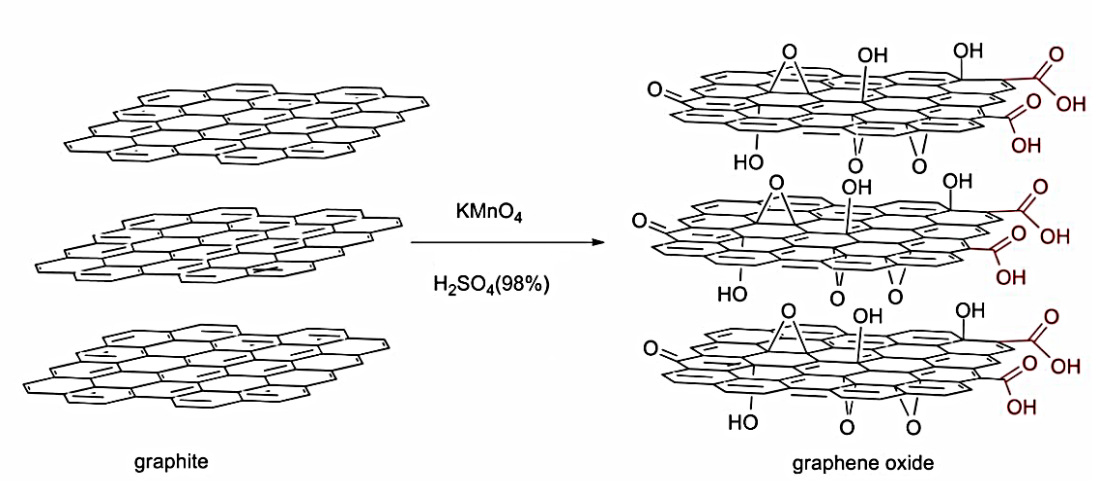

Figure 1.6.4.2 Schematic diagram to produce GO sheets by improved Hummer's Method

1.7 Applications of GO/ FOG

Recent research indicates the implementation of the graphene based materials in various fields as it exhibit greater potential for different applications as chemical sensors [39], nano generators [40], catalysts [41], solar cells [42], photocatalysts [43], hydrogen storage [44] and the most important supercapacitors.

Amongst these applications, FOG-based electrodes made-up for electrochemical performance by low cost and reliable methods have gained greater interest owing to their outstanding properties. For example, rGO sheets having large surface area with potential to substitute (ITO) indium tin oxide in light emitting diodes and touch screens, however, mass production can be attained due to electrical conductivity and its transparency [45, 46]. Furthermore, as compared to the rigid and indium tin oxide, rGO/rGOF is viable in processability and flexibility for assembly of electronic devices.

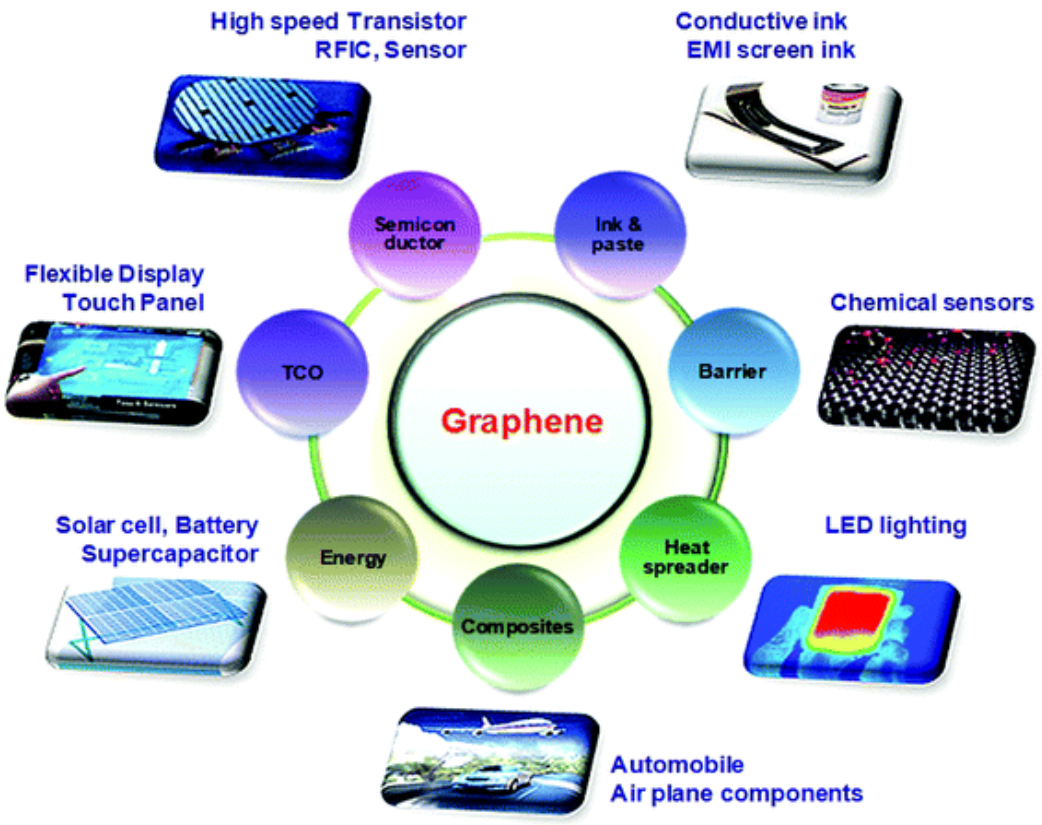

Figure 1.7: The potential applications for graphene and graphene oxide frame works.

1.8 Supercapacitors and Their Properties

Supercapacitor, an electronic device also called ultracapacitors is a high quality capacitor and its capacitance occupy a niche in-between the batteries and simple capacitors. In simple way, we can say that supercapacitors store extra energy than simple capacitor, however, discharges more gradually, and it stores less energy than battery but discharge that energy more quickly. This difference in the performance of supercapacitors originates from the most fundamental and important mechanisms of energy storage every technology, demonstrated in Figure 1.8.

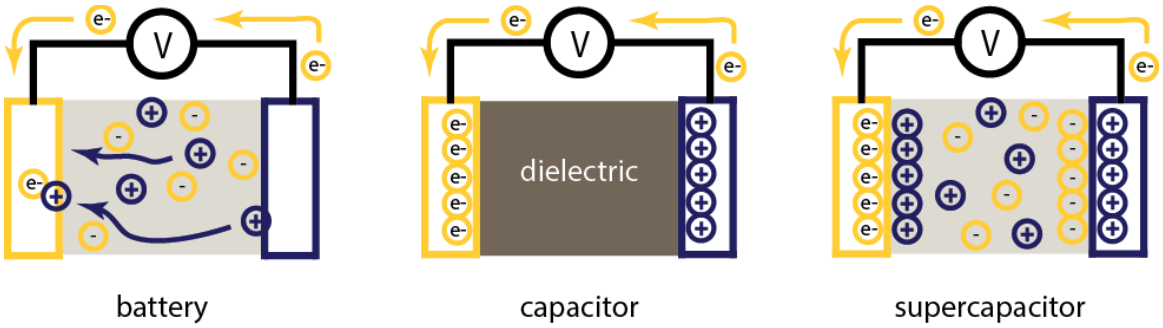

Figure 1.8: Illustration of charge storage mechanism for batteries, capacitors, and supercapacitors.

In capacitors, two electrodes are separated by a superseding dielectric layer. When a potential is applied across the electrodes an equal and opposite charge develops on the both electrodes. However, when a device is powered it introduces a new current path between the two electrodes for the dissipation of charge and thus resultant current can be consumed. In contrast to the capacitors, batteries have two electrodes immersed in an ionically conducting electrolyte. A reversible chemical reaction takes place for the storage of energy on both electrodes. During charging, on one electrode oxidation takes place while on the other electrode reduction occurs, however, on discharging the reactions got reversed. Capacitor works on the principle of electrostatic charge storage without going through chemical reactions whereas batteries undergo chemical reactions to store energy at the two electrodes.

Supercapacitors utilize both the batteries and capacitors principle of energy storage. Supercapacitors like batteries have two electrodes and a conducting electrolyte, however, it stores energy via electrochemical reactions unlike batteries. Upon charging high charge density area develops near the interface by the migration of electrolyte mobile ions to the electrode surface. Nowadays, supercapacitor electrodes are synthesized with wide surface area, leading to more space for charging.

1.8.1 Supercapacitor Theory

The energy storage in supercapacitors occurs at the electrode/electrolyte interface. Two different mechanisms operative in charge storage are:

- Electrostatic double-layer charging
- Faradaic charge transfer (pseudocapacitance)

1.8.1.1 Double-layer Capacitance

Double-layer charging happens when we apply the potential difference across the two electrodes immersed in an ionically conducting electrolyte. The cations move towards one electrode and the anions migrates towards the other electrode. For ideally polarized electrodes, no charge transfer occurs at the electrolyte and electrode; however, this phenomenon produces interfacial areas at both electrodes, where the positive and negative charges in the electrolyte balance charges at the both electrodes.

1.8.1.2 Pseudocapacitance

In contrast to the double layer capacitors, pseudocapacitors store charge at the electrode surface via redox reaction. In an ideal double layer capacitor charge transfer doesn't occur at the interface but in case of pseudocapacitance charge transfer occurs in order to store energy.

For example, in case of ruthenium oxide (RuO_2) electrodes large amounts of charge have been stored through many electron-proton transfer reactions [47, 48]. Reactions given in equation 1.1 and 1.2 have been proposed to describe the mechanism of charge storage.

$$Ru^{4+} + e^{-} \rightarrow Ru^{3+} \qquad \text{Eq 1.1}$$

$$O^{2-} + H^{+} \rightarrow OH^{-} \qquad \text{Eq 1.2}$$

During this reaction electrons are transferred as evident from Eq.1.1; during charging process these electrons move via external circuit (which is attached to the counter electrode) and the current generated from the reverse reaction can be used to execute the electrical work.

This reversible process of charge storage via redox reactions is also named "Faradaic," as compared to the "non-Faradaic" process that regulates double-layer charging.

i. However carbon based electrode storage charges primarily by non-Faradic reactions but overall pseudocapacitance behaviour can be observed for energy storage by three main methods. Surface functionalization is being introducing by reactive species (typically nitrogen and oxygen).

ii. Deposition of the electroactive polymers like polypyrrole and polyaniline.
iii. Deposition of the elctroactive transition metal oxides like MnO_2, RuO_2 etc.

These methods can be used to enhance the overall capacitance up to many folds. As reported when polyaniline was deposited on carbon fibers the gravimetric capacitance increased from 30 Fg^{-1} to 150Fg^{-1}.

1.8.2 Supercapacitor Characterization

In order to characterize and illustrates the electrical performance of supercapacitors, different techniques can be employed. The most important one we have used in our research is three electrode working system.

1.8.2.1 Two vs. Three electrode Measurements

Before a comprehensive argument of electrochemical characterization methods, a comparison should be made amongst two and three electrode systems. As demonstrated in Figure 1.8.2.1, in two electrode measurement assembly which is composed of typically two symmetric electrodes it involves full device measurements. On the other side, in three electrodes working setup, the material needs to be analyzed is measured against the counter and the reference electrode. The counter electrode provides the current required to complete the circuit during measurements. It is usually inert In nature, such as Pt wire. The reference electrode is made up of material with a known oxidation reduction (redox) potential, e.g. the calomel electrode (Hg/Hg_2Cl_2) or $Ag/AgCl_2$ electrode. This reference electrode facilitates the accurate potential measurements at the working electrode. The two electrode working setup is usually used to characterize the entire made-up devices, whereas the three electrode working system is strategic for observing the important electrochemical properties of the working electrode material. The specific capacitance values (in units of Fcm^{-3}, Fcm^{-2}, Fg^{-1}) measured from the two electrode system is typically 4 times less than the three electrode system.

1.8.2.2 Cyclic Voltammetry

Cyclic voltammetry (CV) is a technique in which the potential (V) at the working electrode is swept back and forward at constant rate across a given potential window. The resultant current (I) produced is measured and then plotted against the potential (VA simple description of the potential (V) plotted against time (t) is illustrated in Figure 1.8.2.2.1(a).

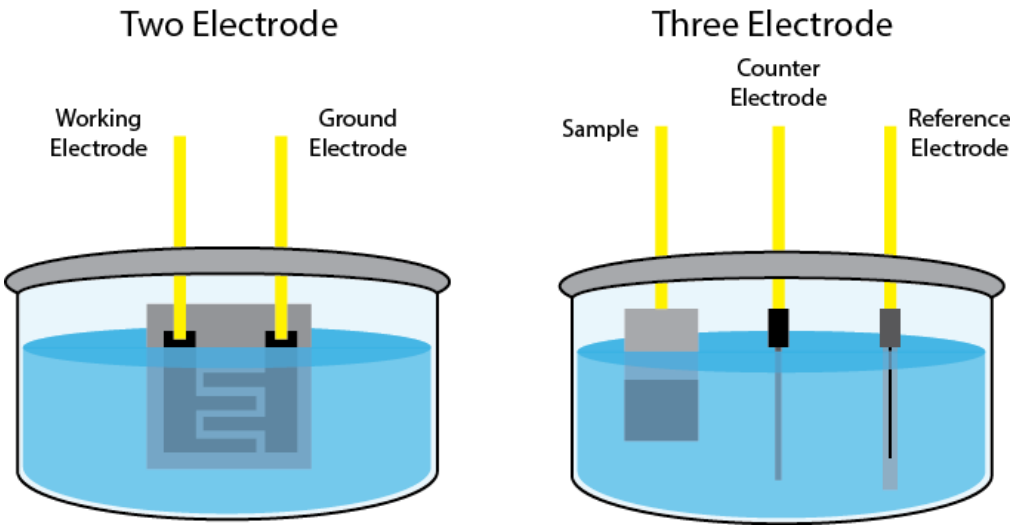

Figure 1.8.2.1: Schematic illustrations of two and three electrode measurements

In the case of ideal supercapacitor, the capacitance remains constant irrespective of the scan rate and it can be calculated the formula given by equation 1.2

$$C = \frac{I}{s} \qquad \text{Eq 1.3}$$

I is the current measured

s is the applied potential scan rate

For an ideal supercapacitor, the resultant current measured is plotted as shown in Figure 1.8.2.2.1 (b, c). When the voltage applied is positive, the resultant current must be positive and along negative voltage sweep the current should be negative constant. Typically, CV plots are presented as in Figure 2.3c, with the current (I) plotted verses the potential (V). In an ideal supercapacitor, the CV plot will be rectangular in shape (symmetric about the zero current axis) and it must follow Eq. 1.2. In reality supercapacitors don't typically exhibit such ideal behaviour but they do it under ideal condition of exceedingly low scan rate.

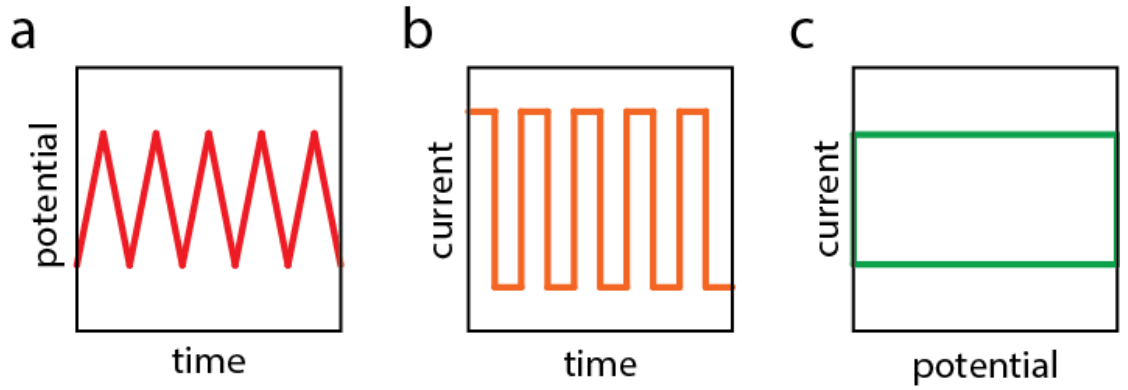

Figure 1.8.2.2.1: a) Cyclic voltammetry potential sweeps plotted vs. time, b) the resulting measured current of an ideal supercapacitor plotted vs. time, c) the CV curve, showing the current plotted vs. potential

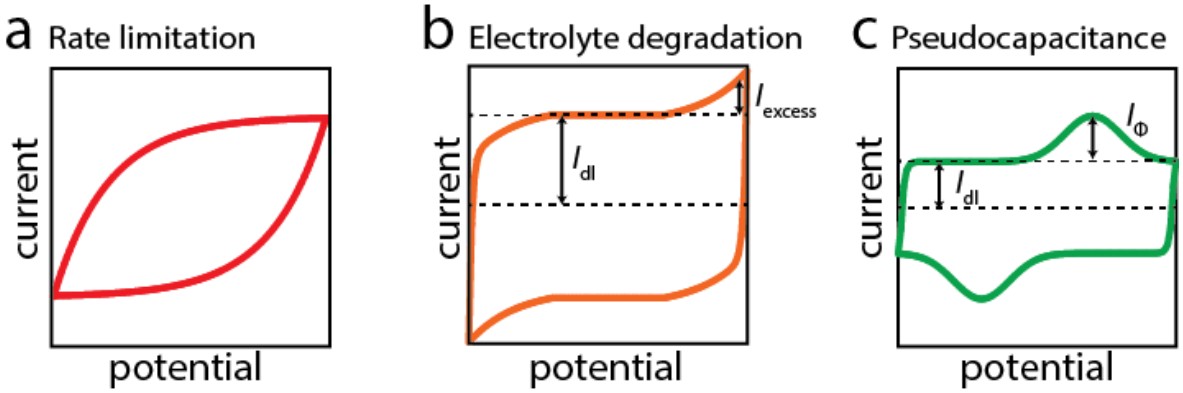

Figure 1.8.2.2.2: Sample supercapacitor CV no idealities: a) sweep rate limitations, b) potential window that exceeds electrolyte stability window, c) pseudocapacitive charge storage

Supercapacitors show non ideal or realistic behaviour at high scan rates. As shown in Figure 1.8.2.2.2(a) the CV plot has specific leaf like shape due to extremely high scan rates, which leads to the rounding off of the corners of the CV plot. This behavior originates from the rate-limiting phenomenon which includes electrolyte ion transport limitations and the limitations of electrical charge transport at the electrode. Because at extremely high scan rates due to transport limitations the interfacial double layer fails to form as it doesn't find much time.

This behavior originates from the rate-limiting phenomenon which includes electrolyte ion transport limitations and the limitations of electrical charge transport at the electrode. Because at extremely high scan rates due to transport limitations the interfacial double layer fails to form as it doesn't find much time.

Electrolyte degradation is another non-ideal behaviour observed in supercapacitor. All electrolytes have a restricted voltage stability window if its value exceeds beyond the limit it undergoes faradic reactions in the electrolyte. For example, potential window of ~ 1 V have been observed in aqueous electrolytes. Moreover, at extremely low or high potentials, water can be easily reduced or oxidized to form hydrogen and oxygen, respectively. These types of reactions, which lead to the transfer of charges across the interface of the electrode and electrolyte, add additional current to the system over that of the only double layer charging current. As shown in Figure 1.8.2.2.2 (b) *I* excess is the current that refers to the electrolyte degradation reactions and not to the charge storage, and while calculating the capacitance (using Eq. 1.2) it should be subtracted. Moreover, the electrolyte degradation can reduce the overall performance of the supercapacitor.

Unlike the current produced due to electrolyte degradation (*I* excess), pseudocapacitive current subsidize the energy storage competences of a device. Capacitive current produced at electrode surface due to faradic reversible reactions; enhance the capacitance due to double-layer charging. Figure 1.8.2.2.2 (c) displays the CV plot of pseudocapacitive system in which *I*Φ represents the capacitive current.

1.8.2.3 Galvanostatic Charge/Discharge

The capacitance of an electrode can be calculated by cyclic voltammetry, however, the galvanostatic charge/discharge technique is often preferred for this purpose [49]. In this technique, a constant charging current is applied until and unless a maximum potential is achieved, at that point discharge current of the same magnitude is applied to reach a minimum potential value. The potential (V) is observed as function of time (t). In CV constant voltage scan rate is used, however, galvanostatic charge/discharge curves use constant current and they may test more accurate performance.

Figure displays some characteristic galvanostatic charge/discharge plots. In an ideal supercapacitor Figure 1.8.2.3(a) the galvanostatic charge and discharge curves must be symmetrical with

throughout a constant slop. The formula given in Eq.1.4 can be used to calculate capacitance

$$C=I\Delta V/\Delta t \qquad \text{Eq 1.4}$$

I is the applied current magnitude

Δ*V*/Δ*t* is the slope of the discharge curve

The capacitance values calculated by using galvanostatic charge/discharge and CV give us the approximately similar values. However, the only difference is that in former numerator is kept constant while denominator is kept constant shown in equation 1.2 and 1.3.

Linear plots are not usually observed in non-ideal conditions in supercapacitors. Such non-ideal behaviour can be observed in Figure 1.8.2.3 (b) due to exceeding electrolyte stability window. The decline in the slop of charge/discharge curves generally shows the charge transfer at the electrolyte/electrode interface. The reactions occur at the electrode and electrolyte give rise to the charge transfer and when the reactions takes place in the electrolyte it leads to its degradation with time and indicates that the reduction of potential window within the limits of the electrolyte stability window.

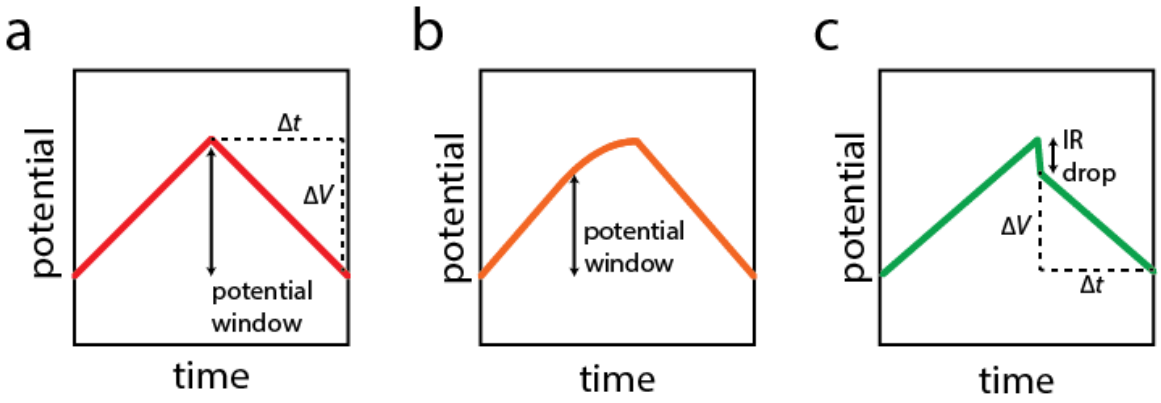

Figure 1.8.2.3 Sample galvanostatic charge/discharge plots. a) An ideal charge/discharge cycle with the slope indicated, b) a charging curve which exceeds the electrolyte stability window, leading to excess charge transfer, c) a discharge curve which is preceded by a large IR potential drop.

On the other hand reversible electrode reactions, could contribute to the charge storage pseudocapacitive behavior; however, irreversible electrode reactions could leads to the

degradation and it damages the electrode so it is undesirable.

Figure 1.8.2.3(c) is the illustrations of another non-ideal behavior observed at very high current density for all supercapacitors. When the capacitor switches from charging to discharging an instantaneous drop in voltage can be measured. This drop in voltage, also term as the IR drop, originates due to the ohmic resistances in the system. The ohmic resistances are the sum of electrolyte resistance, electrode resistance, and any other resistance present in the system.

1.8.2.4 Impedance spectroscopy

The third most commonly used technique to probe supercapacitor material is the Impedance spectroscopy. In this technique, an alternating potential is applied over the wide range of frequencies and the phase shift and the amplitude of the resultant current is measured.

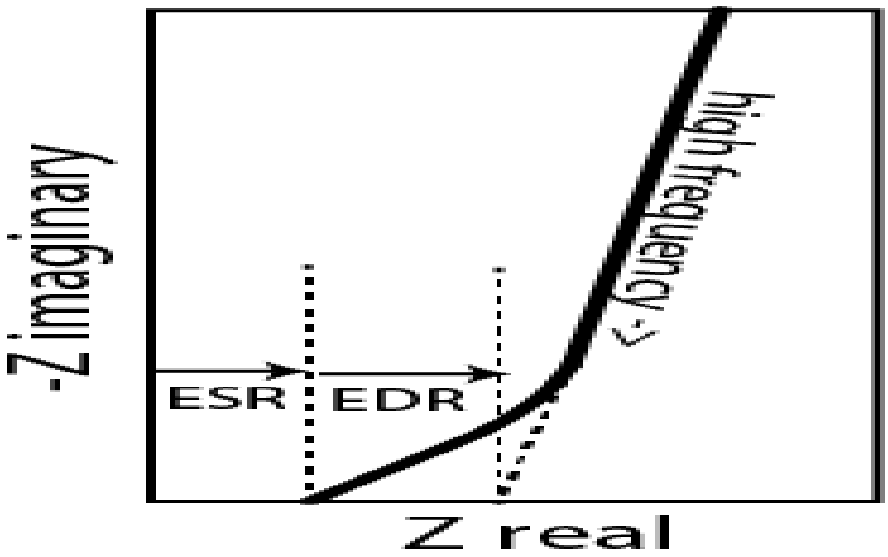

Figure 1.8.2.4: Nyquist plot

Figure: 1.8.2.4 represents the Nyquist plot that exhibits the typical behaviour of the supercapacitor comprising of a porous electrode. In case of ideal RC circuit, the Nyquist plot look like a vertical line at $Z' = R$. The term Z (omega) impedance consists of the both imaginary and the real part. By plotting the real part on the x-axis and imaginary part on the y-axis we will get the Nyquist plot. The semi-circular region in the plot is the characteristic of single RC-constant. Often only a small part of semicircular region becomes visible. A straight line at 45°C region is termed as the Warburg impedance. Whenever the diffusion effect

dominates the electrochemical reaction process the impedance is termed as Warburg impedance. The Warburg impedance becomes small at high frequency as the diffusing reactants not need to move far. However, at low frequency the Warburg impedance increases as the diffusing reactants have to move far.

Present Work

Synthesis of graphene oxide (GO) was carried out by improved Hummer's method. Frame works of graphene oxide were prepared by facial solution method using the para-xylylenediamine (1,4-XDA) and 2,6-diaminopyridine (2,6-DAP) as linkers. Different samples were synthesized by varying the ratio of graphene and linkers. The characterization was done using FT-IR, XRD, TGA, BET and SEM analysis. Electrochemical performance of all synthesized materials has been observed through Cyclic voltammetry, Galvanostatic charge discharge and Electrochemical impedance spectroscopy. Among the all synthesized samples FOG-X-A is proved to be the best material for supercapacitors with C_{sp} value of 360 Fg^{-1}.

References

[1] Chung, D., "Review graphite," *Journal of materials science*, vol. 37(8), pp. 1475-1489, 2002.

[2] Novoselov, K.S., A.K. Geim, S.V. Morozov, D. Jiang, Y. Zhang, S.V. Dubonos, I.V. Grigorieva, and A.A. Firsov, "Electric field effect in atomically thin carbon films," *science*, vol. 306(5696), pp. 666-669, 2004.

[3] Boehm, H.P., R. Setton, and E. Stumpp, "Nomenclature and terminology of graphite intercalation compounds (IUPAC Recommendations 1994),"*Pure and Applied Chemistry*, vol. 66(9), pp. 1893-1901, 1994.

[4] Geim, A.K. and K.S. Novoselov,"The rise of graphene, in Nanoscience and Technology A Collection of Reviews from Nature Journals," *World Scientific*, pp. 11-19, 2010.

[5] Morozov, S., K. Novoselov, M. Katsnelson, F. Schedin, D. Elias, J.A. Jaszczak, and A. Geim,"Giant intrinsic carrier mobilities in graphene and its bilayer," *Physical review letters*, vol. 100(1), pp. 016602, 2008.

[6] Lee, C., X. Wei, J.W. Kysar, and J. Hone,"Measurement of the elastic properties and intrinsic strength of monolayer graphene," *Science*, vol. 321(5887), pp. 385-388, 2008.

[7] Nair, R.R., P. Blake, A.N. Grigorenko, K.S. Novoselov, T.J. Booth, T. Stauber, N.M. Peres, and A.K. Geim, "Fine structure constant defines visual transparency of graphene," *Science,* vol. 320(5881), pp. 1308-1308, 2008.

[8] Zhong, J.-P., Y.-J. Fan, H. Wang, R.-X. Wang, L.-L. Fan, X.-C. Shen, and Z.-J. Shi, "Copper phthalocyanine functionalization of graphene nanosheets as support for platinum nanoparticles and their enhanced performance toward methanol oxidation," *Journal of Power Sources,* vol. 242, pp. 208-215, 2013.

[9] Huang, X., X. Qi, F. Boey, and H. Zhang, "Graphene-based composites," *Chemical Society Reviews*, vol. 41(2), pp. 666-686, 2012.

[10] Huang, Y., J. Liang, and Y. Chen, "An overview of the applications of graphene-based materials in supercapacitors," *Small*, vol. 8(12), pp. 1805-1834, 2012.

[11] Liu, Y., X. Dong, and P. Chen, "Biological and chemical sensors based on graphene materials," *Chemical Society Reviews*, vol. 41(6), pp. 2283-2307, 2012.

[12] Eda, G. and M. Chhowalla, "Chemically derived graphene oxide: towards large-area thin-film electronics and optoelectronics," *Advanced materials*, vol. 22(22), pp. 2392-2415, 2010.

[13] Spyrou, K. and P. Rudolf, "An introduction to graphene,"*Functionalization of graphene*, pp. 1-20, 2014.

[14] Jeong, H.-K., Y.P. Lee, R.J. Lahaye, M.-H. Park, K.H. An, I.J. Kim, C.-W. Yang, C.Y. Park, R.S. Ruoff, and Y.H. Lee, "Evidence of graphitic AB stacking order of graphite oxides," *Journal of the American Chemical Society*, vol. 130(4), pp. 1362-1366, 2008.

[15] LI, L., G. LI, Y. LI, J. GAO, and C. XU, "Preparation of graphene from graphite by supercritical CO 2 exfoliation assisted with fluid shear," *Chinese Science Bulletin,* vol. 60(26), pp. 2561-2566, 2015.

[16] Hummers Jr, W.S. and R.E. Offeman, "Preparation of graphitic oxide," *Journal of the american chemical society*, vol. 80(6), pp. 1339-1339, 1958.

[17] Bourlinos, A.B., D. Gournis, D. Petridis, T. Szabó, A. Szeri, and I. Dékány, “Graphite oxide: chemical reduction to graphite and surface modification with primary aliphatic amines and amino acids,” Langmuir, vol. 19(15), pp. 6050-6055, 2003.

[18] Allen, M.J., V.C. Tung, and R.B. Kaner, “Honeycomb carbon: a review of graphene,” *Chemical reviews*, vol. 110(1), pp. 132-145, 2009.

[19] Lin, Z., M.-k. Song, Y. Ding, Y. Liu, M. Liu, and C.-p. Wong, “Facile preparation of nitrogen-doped graphene as a metal-free catalyst for oxygen reduction reaction,” *Physical Chemistry Chemical Physics*, vol. 14(10), pp. 3381-3387, 2010.

[20] Lu, X., L. Li, B. Song, K.-s. Moon, N. Hu, G. Liao, T. Shi, and C. Wong, “Mechanistic investigation of the graphene functionalization using p-phenylenediamine and its application for supercapacitors,” *Nano Energy*, vol. 17, pp. 160-170, 2015

[21] Chen, P., J.-J. Yang, S.-S. Li, Z. Wang, T.-Y. Xiao, Y.-H. Qian, and S.-H. Yu, “Hydrothermal synthesis of macroscopic nitrogen-doped graphene hydrogels for ultrafast supercapacitor,” *Nano Energy*, vol. 2(2), pp. 249-256, 2013.

[22] Unni, S.M., S. Devulapally, N. Karjule, and S. Kurungot, “Graphene enriched with pyrrolic coordination of the doped nitrogen as an efficient metal-free electrocatalyst for oxygen reduction,” *Journal of Materials chemistry,* vol. 22(44), pp. 23506-23513, 2012.

[23] Li, X., H. Wang, J.T. Robinson, H. Sanchez, G. Diankov, and H. Dai, “Simultaneous nitrogen doping and reduction of graphene oxide,” *Journal of the American Chemical Society*, vol. 131(43), pp. 15939-15944, 2009.

[24] Wu, Z.S., A. Winter, L. Chen, Y. Sun, A. Turchanin, X. Feng, and K. Müllen, “Three-dimensional nitrogen and boron co-doped graphene for high-performance all-solid-state supercapacitors,” *Advanced Materials*, vol. 24(37), pp. 5130-5135, 2012.

[25] Zhang, L.L., Z. Xiong, and X. Zhao, "A composite electrode consisting of nickel hydroxide, carbon nanotubes, and reduced graphene oxide with an ultrahigh electrocapacitance," *Journal of Power Sources,* vol. 222, pp. 326-332, 2013.

[26] Wu, Y., T. Zhang, F. Zhang, Y. Wang, Y. Ma, Y. Huang, Y. Liu, and Y. Chen, "In situ synthesis of graphene/single-walled carbon nanotube hybrid material by arc-discharge and its application in supercapacitors," *Nano Energy*, vol. 1(6), pp. 820-827, 2012.

[27] Yu, G., L. Hu, N. Liu, H. Wang, M. Vosgueritchian, Y. Yang, Y. Cui, and Z. Bao, "Enhancing the supercapacitor performance of graphene/MnO2 nanostructured electrodes by conductive wrapping," *Nano letters*,vol. 11(10), pp. 4438-4442, 2011.

[28] Georgakilas, V., M. Otyepka, A.B. Bourlinos, V. Chandra, N. Kim, K.C. Kemp, P. Hobza, R. Zboril, and K.S. Kim, "Functionalization of graphene: covalent and non-covalent approaches, derivatives and applications," *Chemical reviews*, vol. 112(11), pp. 6156-6214, 2012.

[29] Liu, Z., H. Zhou, Z. Huang, W. Wang, F. Zeng, and Y. Kuang, "Graphene covalently functionalized with poly (p-phenylenediamine) as high performance electrode material for supercapacitors," *Journal of Materials Chemistry A*, vol. 1(10), pp. 3454-3462, 2013.

[30] Wu, J., H. Yu, L. Fan, G. Luo, J. Lin, and M. Huang, "A simple and high-effective electrolyte mediated with p-phenylenediamine for supercapacitor," *Journal of Materials Chemistry*, vol. 22(36), pp. 19025-19030, 2012.

[31] Dreyer, D.R., Sungjin. Park, Christopher W. Bielawski and Rodney S. Ruoff, "The chemistry of graphene oxide," *Chem. Soc. Rev*, vol. 39, pp. 228-240, 2010.

[32] Luo, J., W. Zhong, Y. Zou, C. Xiong, and W. Yang, “Preparation of morphology-controllable polyaniline and polyaniline/graphene hydrogels for high performance binder-free supercapacitor electrodes,” *Journal of Power Sources*, vol. 319, pp. 73-81, 2016.

[33] Fang, M., K. Wang, H. Lu, Y. Yang, and S. Nutt, “Covalent polymer functionalization of graphene nanosheets and mechanical properties of composites,” *Journal of Materials Chemistry,* vol. 19(38), pp. 7098-7105, 2009.

[34] Rosca, I.D., F. Watari, M. Uo, and T. Akasaka, “Oxidation of multiwalled carbon nanotubes by nitric acid*,” Carbon*, vol. 43(15), pp. 3124-3131, 2005.

[35] Becker, L., R.J. Poreda, and T.E. Bunch, “Fullerenes: An extraterrestrial carbon carrier phase for noble gases,” *Proceedings of the National Academy of Sciences*, vol. 97(7), pp. 2979-2983, 2000.

[36] Kovtyukhova, N.I., P.J. Ollivier, B.R. Martin, T.E. Mallouk, S.A. Chizhik, E.V. Buzaneva, and A.D. Gorchinskiy, “Layer-by-layer assembly of ultrathin composite films from micron-sized graphite oxide sheets and polycations,” *Chemistry of materials,* vol. 11(3), pp. 771-778, 1999.

[37] Marcano, D.C., D.V. Kosynkin, J.M. Berlin, A. Sinitskii, Z. Sun, A. Slesarev, L.B. Alemany, W. Lu, and J.M. Tour, “Improved synthesis of graphene oxide,” ACS nano, vol. 4(8), pp. 4806-4814, 2010.

[38] Chen, J., B. Yao, C. Li, and G. Shi, “An improved Hummers method for eco-friendly synthesis of graphene oxide,” *Carbon,* vol. 64: pp. 225-229, 2013.

[39] Robinson, J.T., F.K. Perkins, E.S. Snow, Z. Wei, and P.E. Sheehan, “Reduced graphene oxide molecular sensors,” *Nano letters,* vol. 8(10), p. 3137-3140, 2008.

[40] Choi, D., M.Y. Choi, W.M. Choi, H.J. Shin, H.K. Park, J.S. Seo, J. Park, S.M. Yoon, S.J. Chae, and Y.H. Lee, "Fully rollable transparent nanogenerators based on graphene electrodes," *Advanced Materials,* vol. 22(19), pp. 2187-2192, 2010.

[41] Li, Y., X. Fan, J. Qi, J. Ji, S. Wang, G. Zhang, and F. Zhang, "Palladium nanoparticle-graphene hybrids as active catalysts for the Suzuki reaction," *Nano Research*, vol. 3(6), pp. 429-437, 2010.

[42] Wu, J., H.A. Becerril, Z. Bao, Z. Liu, Y. Chen, and P. Peumans, "Organic solar cells with solution-processed graphene transparent electrodes," *Applied Physics Letters*, vol. 92(26), pp. 237, 2008.

[43] Zhang, H., X. Lv, Y. Li, Y. Wang, and J. Li, "P25-graphene composite as a high performance photocatalyst," *ACS nano*, vol. 4(1), pp. 380-386, 2009.

[44] Dimitrakakis, G.K., E. Tylianakis, and G.E. Froudakis, "Pillared graphene: a new 3-D network nanostructure for enhanced hydrogen storage," *Nano letters*, vol. 8(10), p. 3166-3170, 2008.

[45] Kim, K.S., Y. Zhao, H. Jang, S.Y. Lee, J.M. Kim, K.S. Kim, J.-H. Ahn, P. Kim, J.-Y. Choi, and B.H. Hong, "Large-scale pattern growth of graphene films for stretchable transparent electrodes," *nature*, vol. 457(7230), pp. 706, 2009.

[46] Bae, S., H. Kim, Y. Lee, X. Xu, J.-S. Park, Y. Zheng, J. Balakrishnan, T. Lei, H.R. Kim, and Y.I. Song, "Roll-to-roll production of 30-inch graphene films for transparent electrodes," *Nature nanotechnology*, vol. 5(8), pp. 574, 2010.

[47] Conway, B., "Electrochemical Capacitors: Scientific Fundamentals and Technology Applications," *Springer*, 1999.

[48] Conway, B., V. Birss, and J. Wojtowicz, “The role and utilization of pseudocapacitance for energy storage by supercapacitors,” *Journal of Power Sources,* vol. 66(1-2), pp. 1-14, 1997.

[49] Stoller, M.D. and R.S. Ruoff, “Best practice methods for determining an electrode material's performance for ultracapacitors,” *Energy & Environmental Science*, vol. 3(9), pp. 1294-1301, 2010.

Chapter 2 Experimental

2.1 Reagent and Chemicals

Chemicals	Make	Chemicals	Make	Chemicals	Make
Graphite Powder	Sigma Switzerland	Sulphuric acid	Lab Scan Thailand	Potassium Permagnate	Merck Germany
Hydrogen Peroxide	Merck Germany	Para-Xylylenediamine (1,4-XDA)	Sigma Japan	2,6-Diaminopyridine (2,6-DAP)	Fluka
Hydrazine Hydrate	Merck Germany	Absolute Ethanol	BDH England	Hydrochloric Acid	Lab Scan Thailand
Deionized Water	Lab Grade	Distilled Water	Lab Grade	Nylon Filter Paper 0.45 µm 47 mm	Sartorius Germany

2.2 Apparatus and Instruments

Instruments	Make	Instruments	Make	Instruments	Make
Centrifuge Machine	Hermle Labortechik	Sonication Bath	Elmasonic E30-H Germany	Filtration Assembly	Millipore Germany
Vacuum Oven	Memmet Germany	FTIR Analyzer	BRUKER Germany	UV Spectrophotometer	BMS UV 2800
X-Ray Powder Diffraction (XRPD)	STOE Germany	Thermo gravimetric Analyzer (TGA)	Shimadzu's USA	Scanning Electron Microscopy (SEM)	Mira
Brunauer- Emmett-Teller (BET)		Cyclic Voltammetry			

2.3 Synthesis of Graphene Oxide (GO)

Graphene oxide (GO) was synthesized by "Modified Hummers„ method" in which a beaker was placed on ice-bath set temperature ≤ 5 °C, followed by the addition of 140 ml conc. H_2SO_4 in it. Addition of 3 g of graphite powder in to it with stirring until complete dispersion. Slowly bit by bit addition of 9 g of $KMnO_4$ in the dispersion to maintained the temperature ≤ 15 °C, for 6 h. Then distilled water (140 ml) was slowly added below 90 °C. After stirring for 1 h 420 ml of distilled water and 30 ml of H_2O_2 were added on continuous stirring overnight. Reaction mixture poured in falcon tube and centrifuge at 8000 rpm for 3 hours (2 times with water and one time with 5% HCl washing) to separate the precipitated product. The obtained product was dried in vacuum oven for 24 hours at 60°C; the dried product was 2.104g (70.13%)

yield [1, 2].

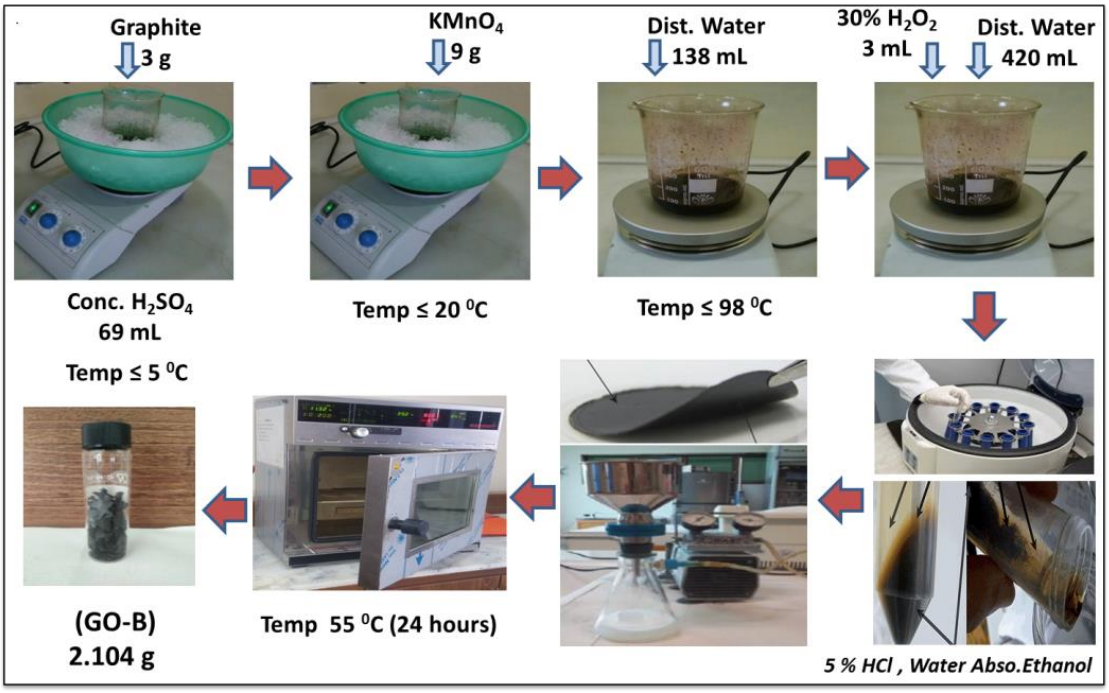

Figure 3.1 GO Synthesis

2.4 Synthesis of Functionalized Graphene Oxide Frameworks (FOG)

Graphene oxide dispersion prepared by dissolving 300 mg GO into 150 ml deionized water and sonicates it for 60 minutes. 300 mg Linker molecules (Para-Xylyenediamine and 2, 6-Diamino Pyridine) dissolved into 150 ml deionized water; pour this mixture into GO dispersion slowly by continuous stirring. The above dispersion sonicate for 60 minutes and placed in round bottom flask heating on oil bath at 80 °C with continuous stirring for 1 day. Addition of Hydrazine Hydrate (10 ml) to the above dispersion drop wise and shifted the dispersion for reflux at 90 °C for 12 hours. Mixture cooled at room temperature and washed with deionized water through flirtation assembly, the obtained product dried in vacuum oven at 60 °C for 24 hours [3, 4]. Similarly as above three different concentration of GO: Linker dispersion ratios have been prepared.

Sr.	GO: Para-Xylyenediamine (PXDA)	GO: 2,6-Diaminopyridine (DAP)
1.	0.5:1	0.5:1
2.	1:1	1:1
3.	1:1.5	1:1.5

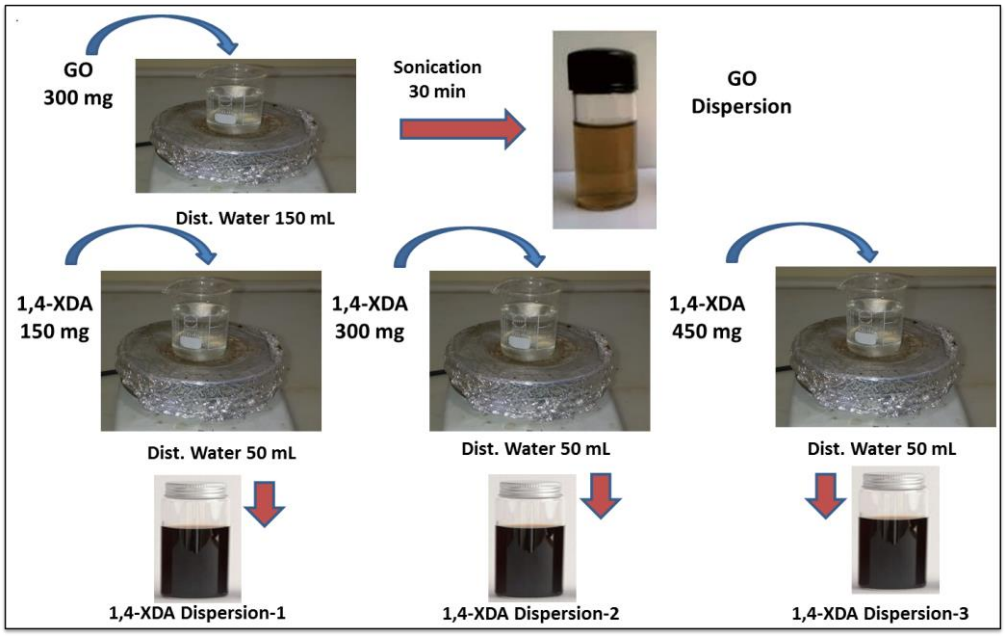

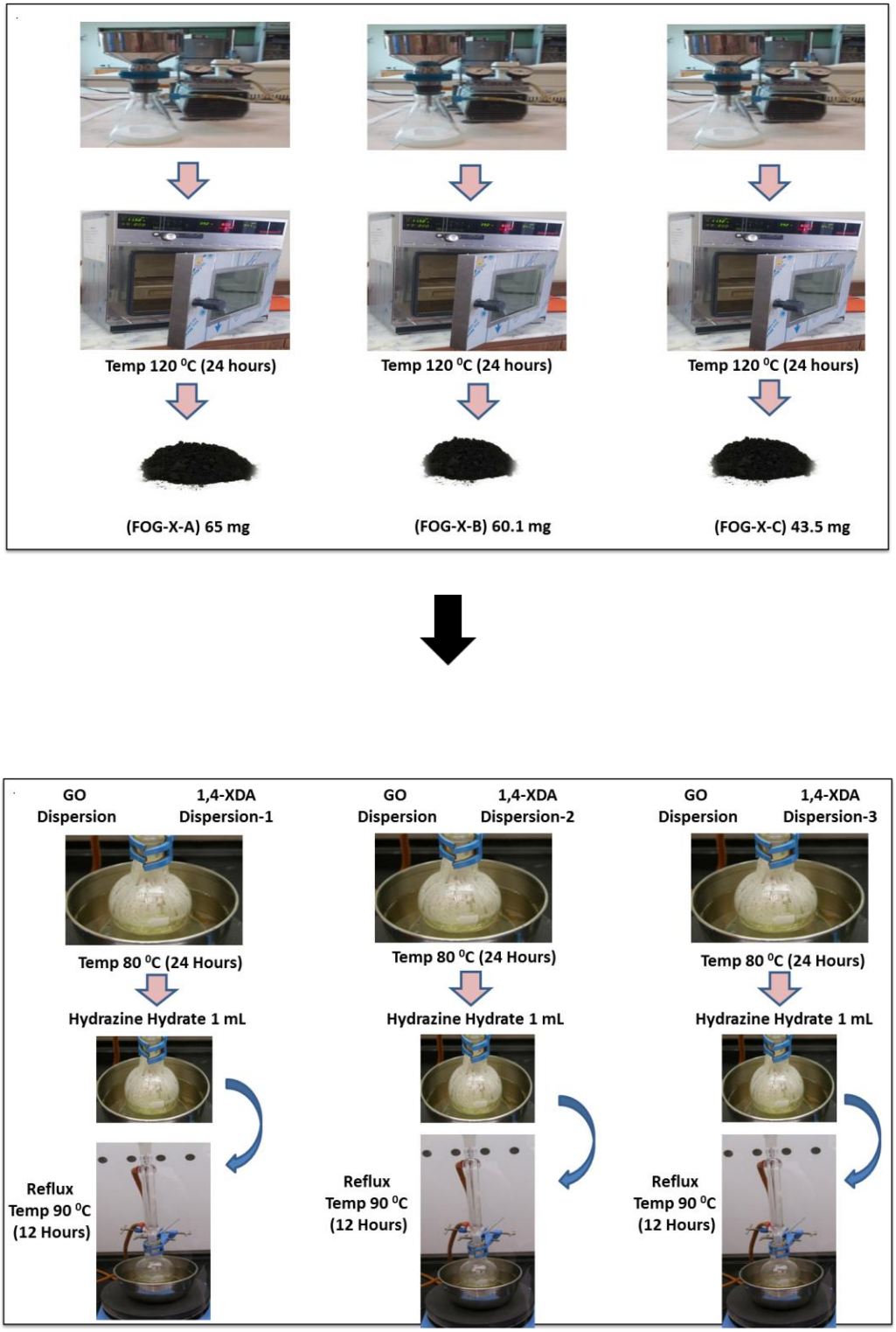

Figure 3.2 FOG Synthesis

References:

[1] J. Chen, B. Yao, C. Li, and G. Shi, "An improved Hummers method for eco-friendly synthesis of graphene oxide," *Carbon,* vol. 64, pp. 225-229, 2013.

[2] D. C. Marcano, D. V. Kosynkin, J. M. Berlin, A. Sinitskii, Z. Sun and A. Slesarev, "Improved Synthesis of Graphene Oxide," *ACS Nano,* vol. 4, pp. 4806-4814, 2010.

[3] X. Lu, L. Li, B. Song, K.-s. Moon, N. Hu and G. Liao., "Mechanistic investigation of the graphene functionalization using p -phenylenediamine and its application for supercapacitors," *Nano Energy,* vol. 17, pp. 160-170, 2015.

[4] B. Feng, K. Xu, and A. S. Huang, "Covalent synthesis of three-dimensional graphene oxide framework (GOF) membrane for seawater desalination," *Desalination,* vol. 394, pp. 123-130, Sep 15 2016.

Chapter 3 Results and Discussion

3.1 FTIR Analysis

3.1.1 FTIR of Graphite and GO

Atomic vibration in molecules provides information about functional groups in material that was obtained through FTIR technique. Figure 3.1.1.1 show the FTIR spectra of graphite powder that is featureless, no functional groups present in graphite, while in Figure 3.1.1.2 the GO spectrum shows different bands in the range of 4000-600 cm^{-1} that is confirmation of GO formation, these bands are due to different groups present on surface of GO [1, 2].

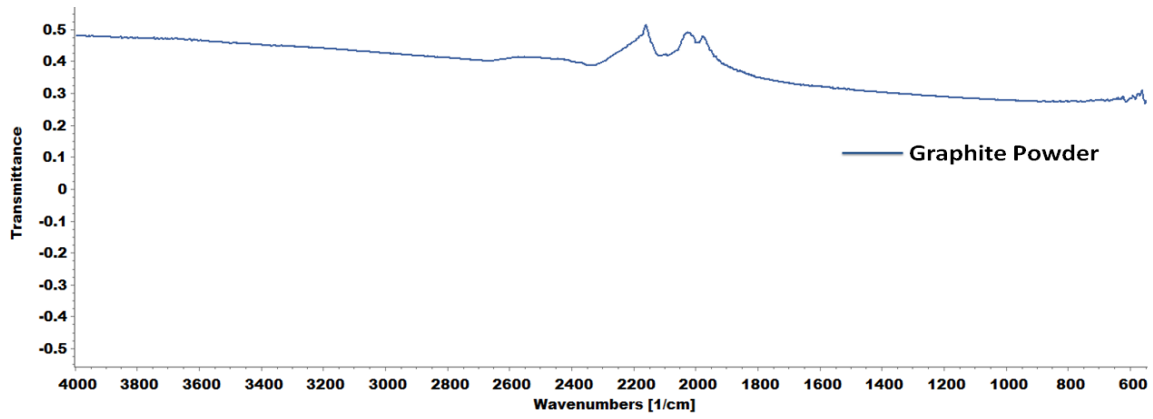

Figure 3.1.1.1 FTIR Spectrum of Graphite

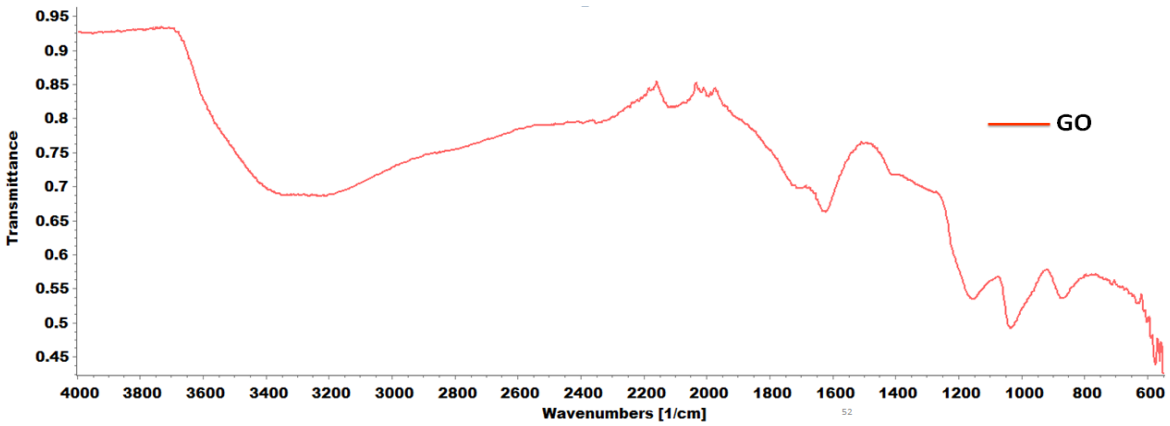

Figure 3.1.1.2 FTIR Spectrum of GO

Table 3.1.1 FTIR of GO

Bands	930 cm^{-1}	1043 cm^{-1}	1220 cm^{-1}	1620 cm^{-1}	1720 cm^{-1}	3258 cm^{-1}
	C-O Shoulder Str	C-O Str	C-O-C Str	C=C Str	C=O Str	O-H Str

3.2 XRD Analysis

3.2.1 XRD of Graphite and GO

XRD technique mostly used for characterization of crystalline type materials from which we obtained information about d-spacing between the layers of material. Graphite XRD show peak (002) at 2θ ~ 26.54 with d spacing 3.33 A°, while the GO having new peak (001) at 2θ ~ 10.37 with d spacing 8.71 A°. Peak value shifting to lower 2θ with enhancing d-spacing is in the favor of GO confirmation, also peak intensity lower in GO as compared to graphite and peak broadening in GO as compared to graphite, as shown in Figure 3.2.1 [3, 4].

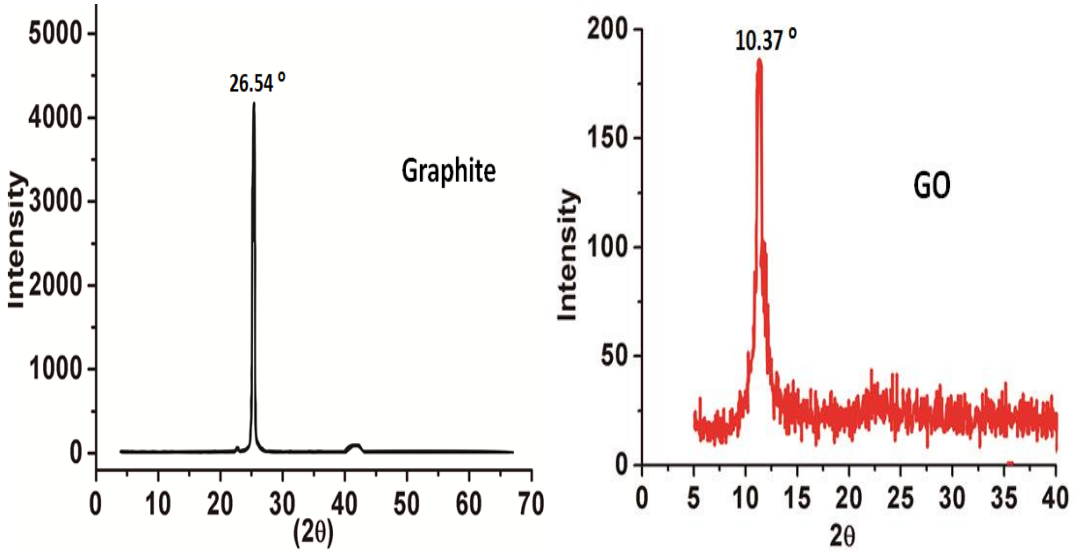

Figure 3.2.1 XRD of Graphite and GO

Table 3.2.1 XRD of Graphite and GO

Sr #	Sample	2θ	d-Spacing A°	Peak Intensity
1.	Graphite Powder	26.54	3.33	4150
2.	Graphene Oxide (GO)	10.37	8.71	183

3.3 TGA Analysis

3.3.1 TGA of Graphite and GO

TGA technique is used to find the thermal stability of materials, the graphite have only 5.3 % weight loss up to 700 °C due to removal of absorbed moisture of graphite powder. In GO having 11.5 % weight loss due to the trapped water molecules on the surface of GO , 25.6 % weight loss up to 200 °C due to loss of less stable oxygen containing functional groups like epoxy and 47.3 % weight loss above 300 °C due to pyrolysis of most stable functional groups like carbonyl as shown in Figure 3.3.1 [5, 6].

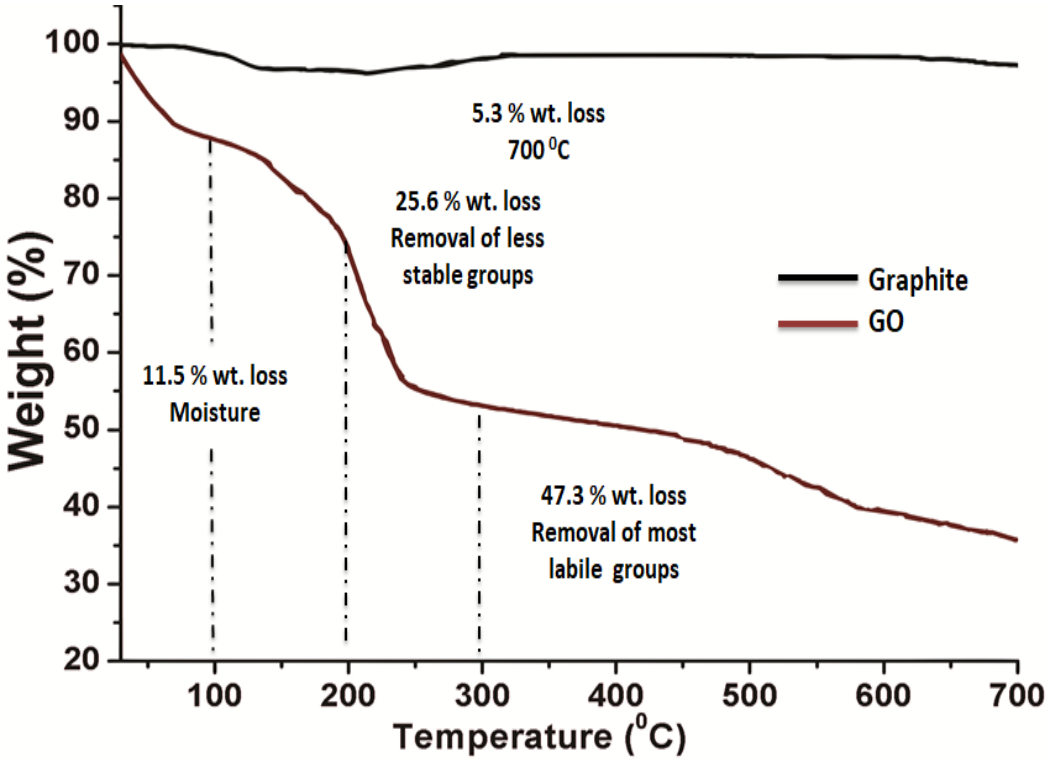

Figure 3.3.1 TGA of Graphite and GO

3.4 SEM Analysis

3.4.1 SEM of Graphite and GO

SEM analysis of graphite and GO at different magnification like (100 µm, 50 µm, 10 µm, 5 µm and 0.5 µm) is shown in the Figure 3.4.1. Graphite powder have layers firmly stacked and closed together while in GO layers are loosely stacked with disorder and corrugation, similarly in GO sheets looks like crumped having enhanced spacing between them [7] [8].

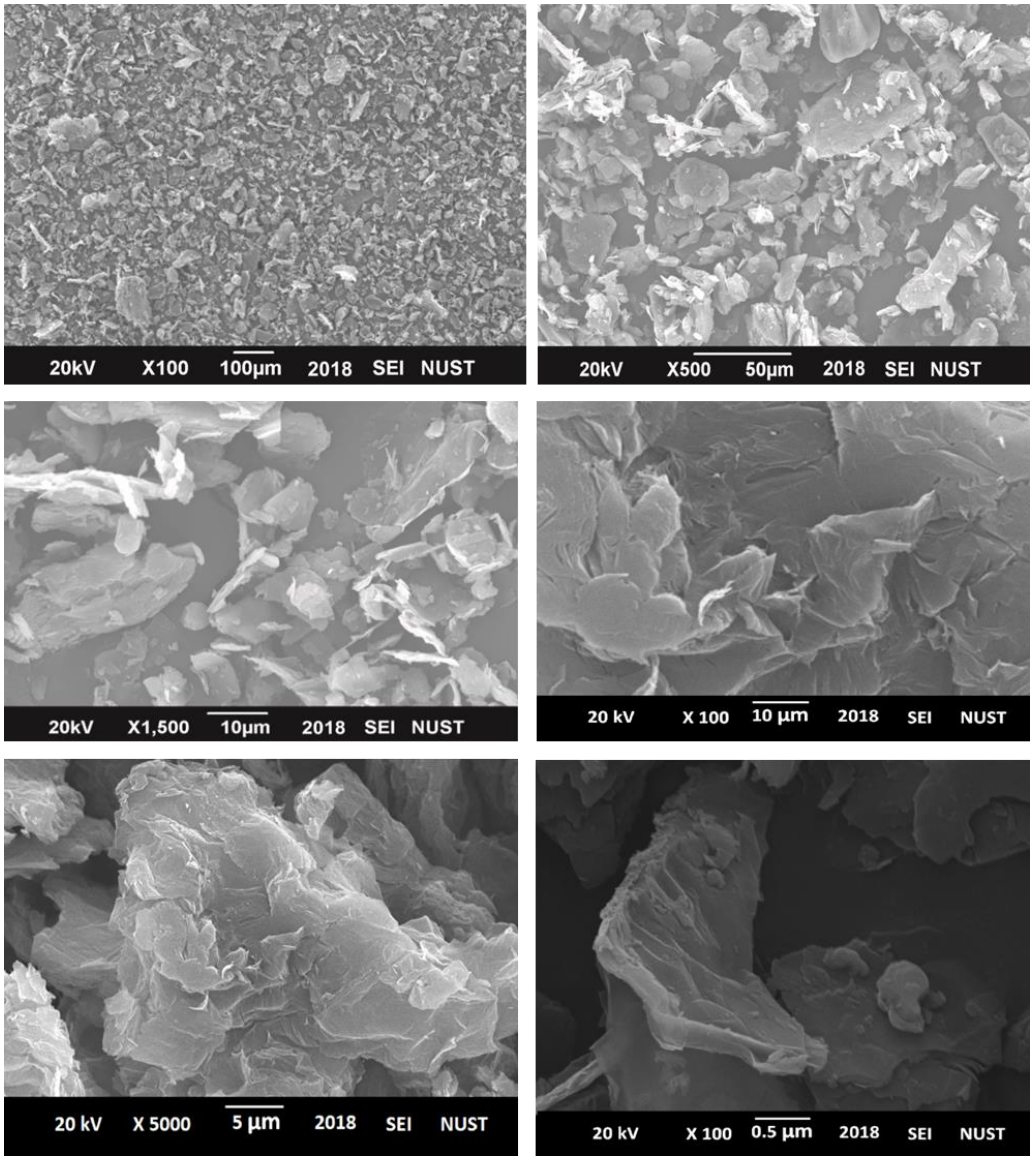

Figure 3.4.1 SEM of Graphite and GO

3.5 FTIR of Para-Xylylenediamine (1, 4-XDA)

1,4-XDA linker molecule having peak at different region in FTIR spectrum, shown characteristic primary amine peaks at 3405 and 3361 cm^{-1} , similarly also shown the di-substituted benzene ring peak at 831 cm^{-1} as shown in the Figure 3.5.1 and described in table 3.5.1 .

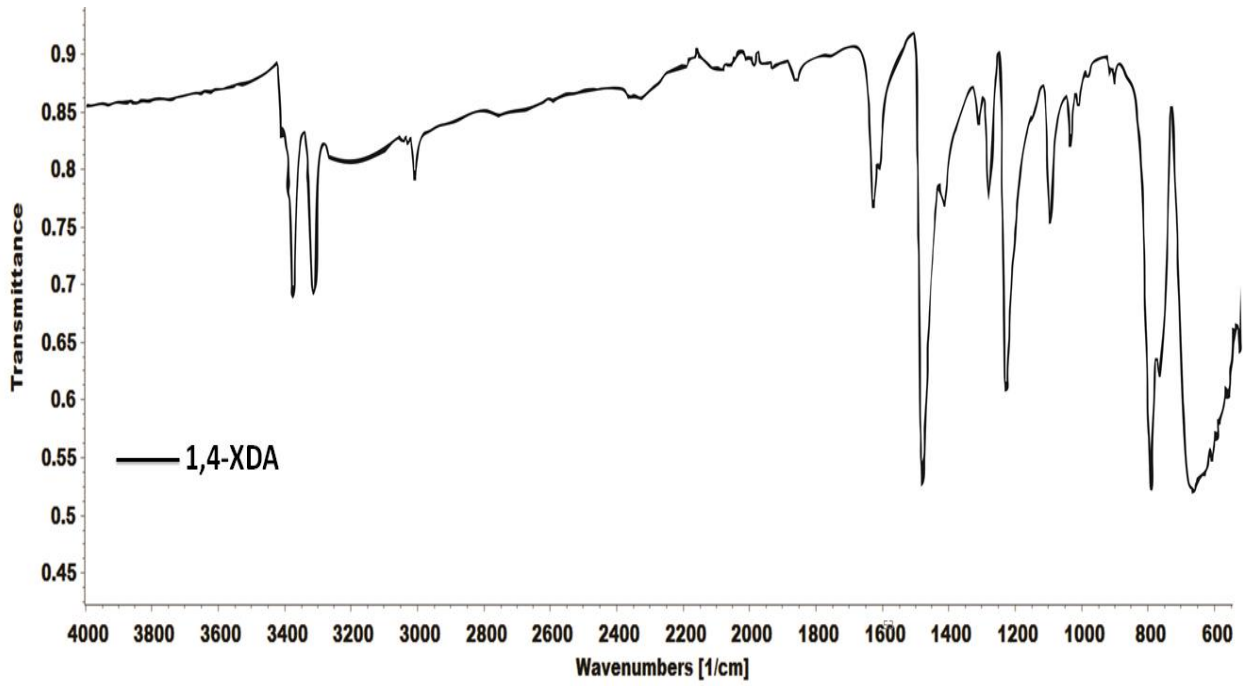

Figure 3.5.1 FTIR Spectrum of 1, 4-XDA

Table 3.5.1 FTIR of 1, 4-XDA

Bands	3405 and 3361 cm^{-1}	3003 cm^{-1}	1621 cm^{-1}	1501 cm^{-1}
	Primary amine $–NH_2$	C-H Str	C-N ben	Aromatic Str
Bands	1216 cm^{-1}	1112 and 1060 cm^{-1}	831 cm^{-1}	705 cm^{-1}
	C-N-C ben	C-H def	Di-Subs	C-H ben

3.6 FTIR of 2, 6-Diaminopyridine (2, 6-DAP)

2,6-DAP linker molecule having peak at different region in FTIR spectrum, have characteristic primary amine peaks at 3345 and 3218 cm^{-1} as shown in the Figure 3.6.1 and described in table 3.6.1.

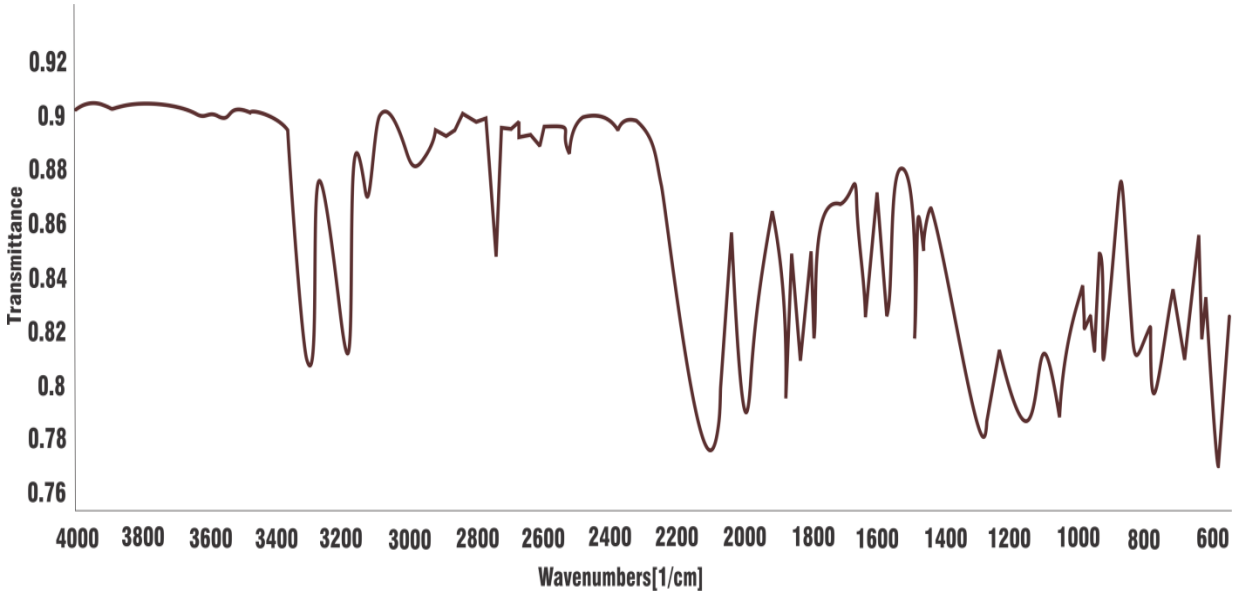

Figure 3.6.1 FTIR Spectrum of 2, 6-DAP

Table 3.6.1 FTIR of 2, 6-DAP

Bands	3345 and 3218 cm^{-1}	2778 cm^{-1}	2128 cm^{-1}	1228 cm^{-1}
	Primary amine $–NH_2$	C-H Str	C-N-H ben	Aromatic Str
Bands	1420 cm^{-1}	1360 cm^{-1}	1167 and 1071 cm^{-1}	814 cm^{-1}
	C-N Str	C-N-C ben	C-H def	C-H ben

3.7 FOG FTIR Analysis

3.7.1 FOG-X-A

FOG-X-A framework showed bands at different region in FTIR spectrum, with characteristic vibrations secondary amine peaks at 3329 cm^{-1} indicating the attachment of linker molecule with GO , C=O peak at 1621 cm^{-1} is also indication of framework formation as shown in the Figure 3.7.1 and described in Table 3.7.1 [9, 10].

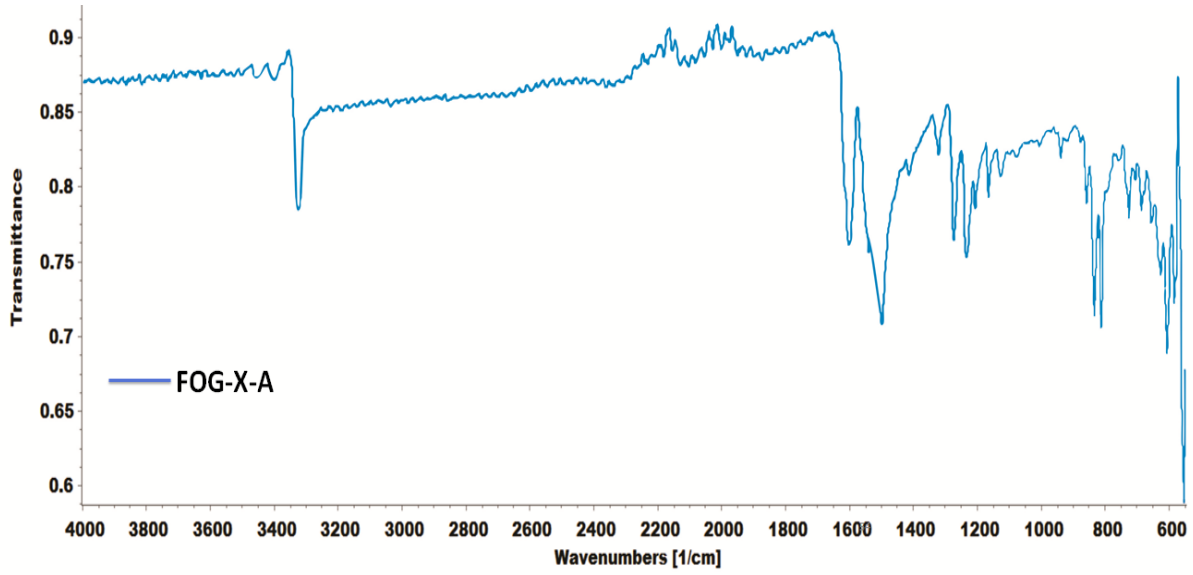

Figure 3.7.1 FTIR Spectrum of FOG-X-A

Table 3.7.1 FTIR of FOG-X-A

Bands	3329 cm^{-1}	1621 cm^{-1}	1506 cm^{-1}	1244 cm^{-1}
	Secondary amine –NH	C=O Str	C=C Aromatic Str	C-N-C Str
Bands	834 cm^{-1}	815 cm^{-1}		
	Di-Subs	N-H Weg		

3.7.2 FOG-X-B

FOG-X-B framework showed bands at different region in FTIR spectrum, with characteristic vibrations at 3440 and 3332 cm^{-1} these are due to either primary and secondary amine , in this framework some side have attached proper with GO to form secondary linkage and some side have no available groups for intercalation they remain as primary amine , it show also C=O band at 1623 cm^{-1} as shown in the Figure 3.7.2 and described in Table 3.7.2 [11].

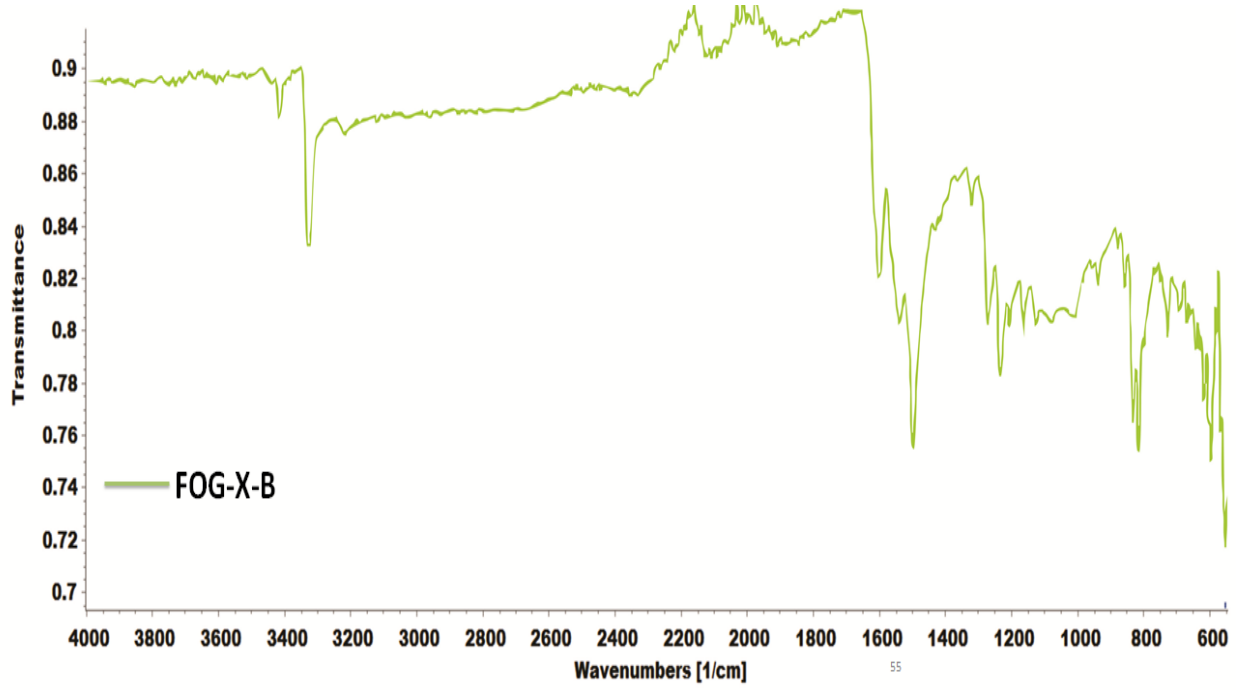

Figure 3.7.2 FTIR Spectrum of FOG-X-B

Table 3.7.2 FTIR of FOG-X-B

Bands	3440 cm^{-1}	3332 cm^{-1}	1623 cm^{-1}	1511 cm^{-1}
	Primary amine $-NH_2$	Secondary amine $-NH_2$	C=O Str	C=C Aromatic Str
Bands	1241 cm^{-1}	834 cm^{-1}		
	C-N-C Str	Di-Subs		

3.7.3 FOG-X-C

FOG-X-C framework gave vibrations at different region in FTIR spectrum, without characteristic bands in the region of primary and secondary amine , because as the concentration of linker molecules increased reduced the GO, they showed C=O band at 1655 cm^{-1} and C-O epoxy at 982 cm^{-1} as shown in the Figure 3.7.3 and described in Table 3.7.3 [10].

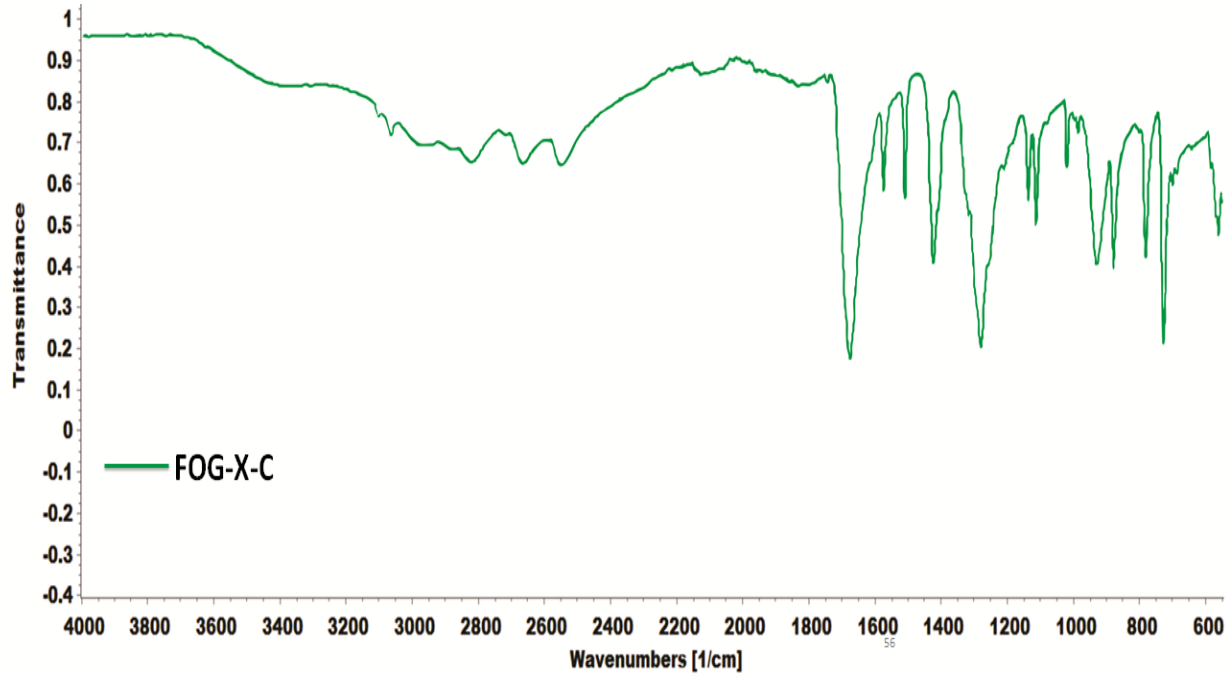

Figure 3.7.3 FTIR Spectrum of FOG-X-C

Table 3.7.3 FTIR of FOG-X-C

Bands	1655 cm^{-1}	1411 cm^{-1}	1289 cm^{-1}	982 cm^{-1}
	C=O Str	C-N Str	C-N-C Str	C-O Str

3.7.4 FOG-D-A

FOG-D-A framework having bands at different region in FTIR spectrum, have characteristic secondary amine bands at 3342 cm^{-1} is indication for proper linkage of linker molecule in GO layers , similarly shown C=O band at 1605 cm^{-1} and benzene di-substituted vibration at 831 cm^{-1} are given in the Figure 3.7.4 and described in Table 3.7.4 [9].

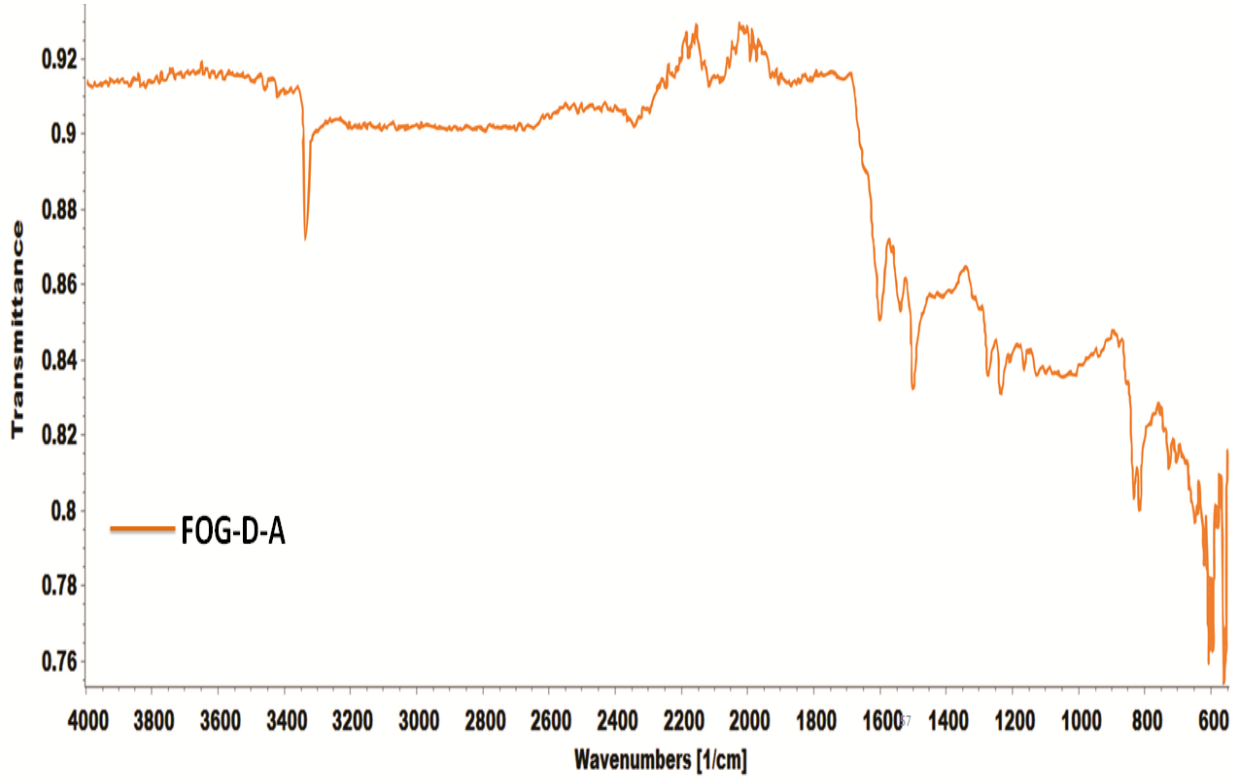

Figure 3.7.4 FTIR Spectrum of FOG-D-A

Table 3.7.4 FTIR of FOG-D-A

Bands	3342 cm^{-1}	1601 cm^{-1}	1511 cm^{-1}	1291 cm^{-1}
	Secondary amine –NH	C=O Str	C=C Aromatic Str	C-N Str
Bands	1241 cm^{-1}	831 cm^{-1}		
	C-N-C Str	Di-Subs		

3.7.5 FOG-D-B

FOG-D-B framework having peak at different region in FTIR spectrum, have no characteristic peaks in the region of above 3000 cm^{-1} so there is no primary nor secondary amine peak the linker molecule reduced the GO as shown in the figure 3.7.5 and described in table 3.7.5 [12].

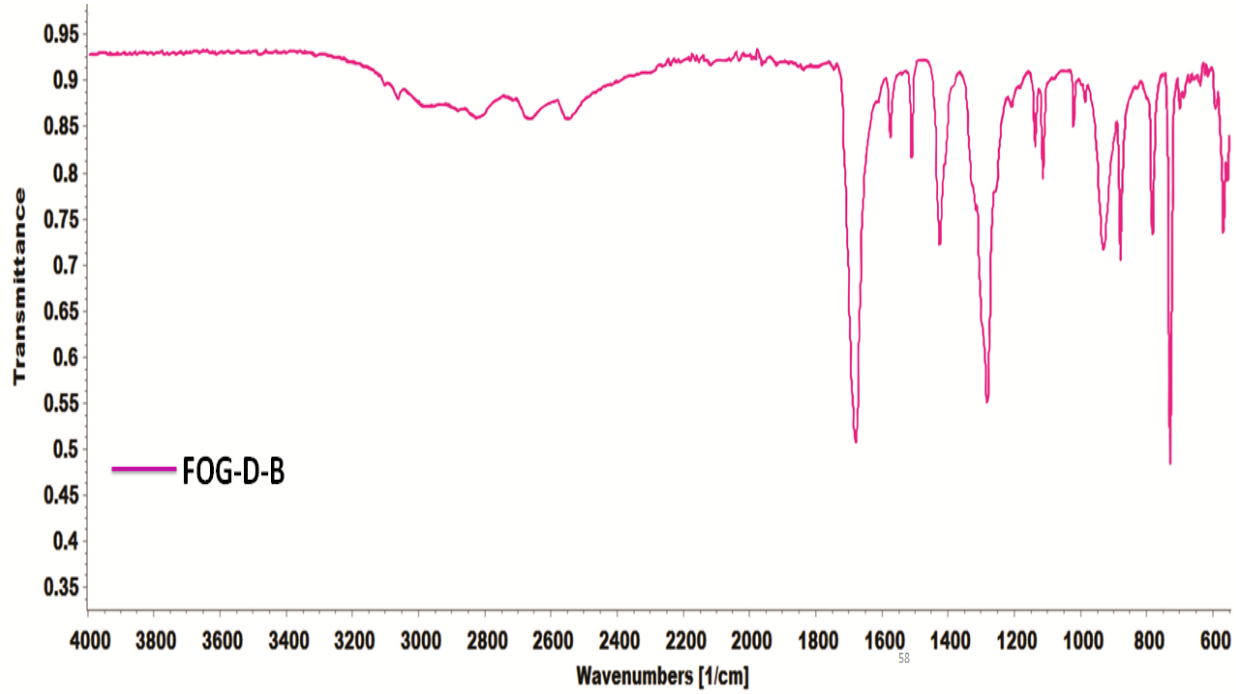

Figure 3.7.5 FTIR Spectrum of FOG-D-B

Table 3.7.5 FTIR of FOG-D-B

Bands	1691 cm^{-1}	1434 cm^{-1}	1278 cm^{-1}	914 cm^{-1}
	C=O Str	C-N Str	C-O-C Str	C-O Str

3.7.6 FOG-D-C

The FTIR spectrum of FOG-D-C framework gave no characteristic primary and secondary amine bands and it have reduced graphene as shown in the Figure 3.7.6 and described in Table 3.7.6 [10, 12].

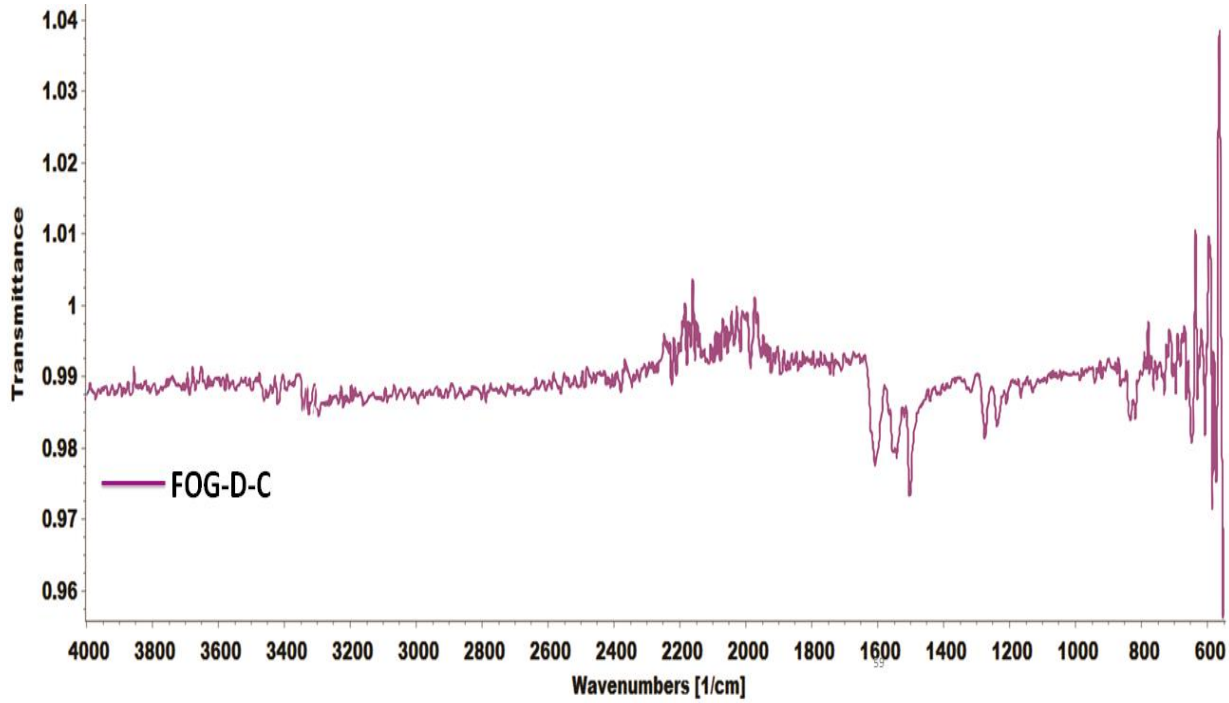

Figure 3.7.6 FTIR Spectrum of FOG-D-C

Table 3.7.6 FTIR of FOG-D-C

Bands	1604 and 1511 cm^{-1}	1221 cm^{-1}	813 cm^{-1}	
	C=C Aromatic Str	C-O Str	N-H	

3.8 FOG XRD

3.8.1 XRD of FOG-X-A, FOG-X-B and FOG-X-C

GO reacting with 1,4-XDA to form (FOG-X-A) framework having 2θ peak shifting to lower value at 7.17, having decreased intensity and also broadening of peak is evidence for formation of framework. Framework (FOG-X-B) have small peak at 2θ~ 7.86 having 145 intensity, similarly for framework (FOG-X-C) have small peak around 2θ~8.49. From all these the framework FOG-X-A is proper linkage of 1,4-XDA intercalation with GO [9, 13, 14].(Figure 3.8.1)

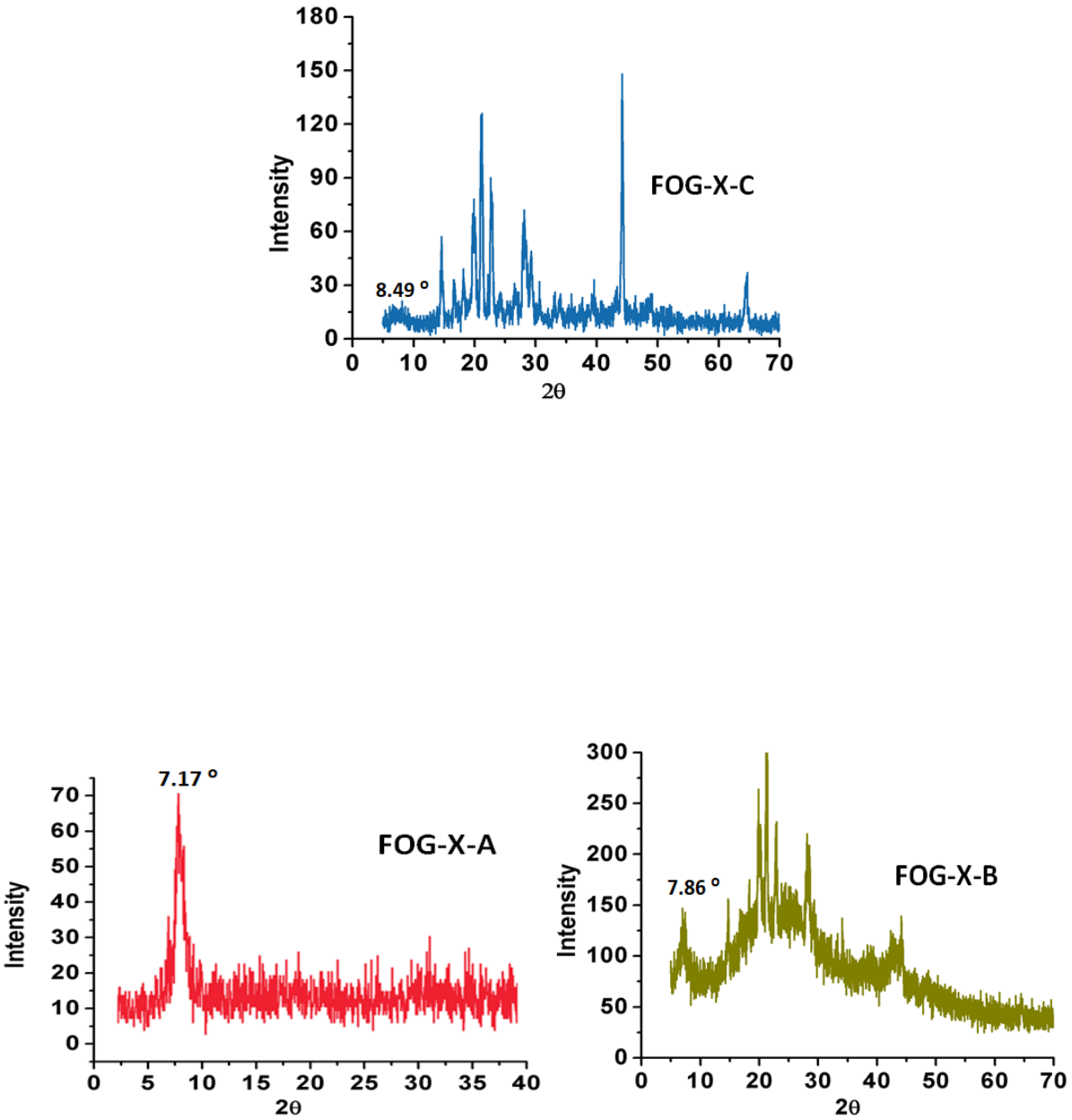

Figure 3.8.1 XRD of FOG-X-A, FOG-X-B and FOG-X-C

3.8.2 XRD of FOG-D-A, FOG-D-B and FOG-D-C

GO reacting with 2,6-DAP to form (FOG-D-A) framework having 2θ peak shifting to lower value at 7.34 with decreased intensity and also broadening of peak is the evidence for the formation of framework. Framework (FOG-D-B) has no peak in the range of $2\theta \leq 10$, similarly for framework (FOG-X-C) have no peak in the range of $2\theta \leq 10$. From all these the framework FOG-D-A is proper linkage of 2,6-DAP intercalation with GO [9, 13, 14].

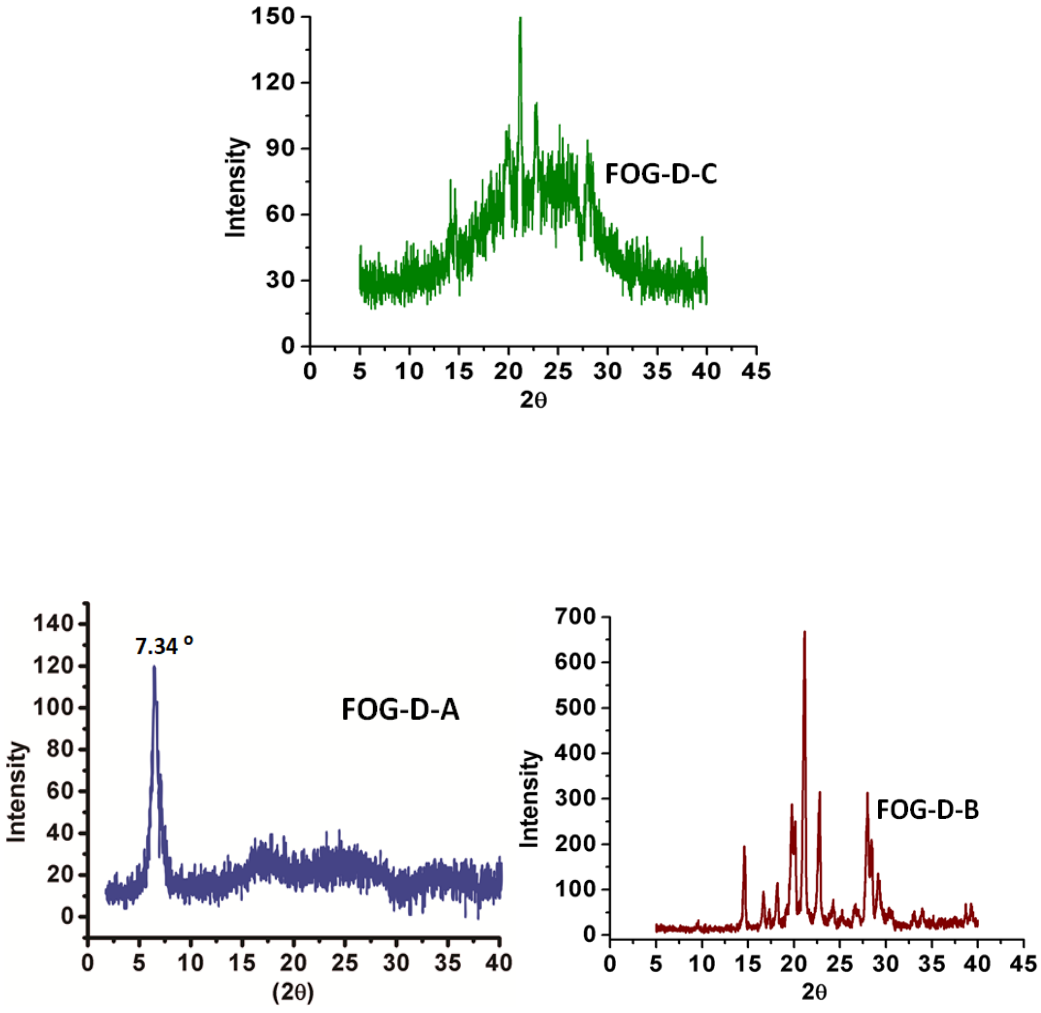

Figure 3.8.2 XRD of FOG-D-A, FOG-D-B and FOG-D-C

Table 3.8.2 Table of XRD

Sr #	Sample	2θ	d-Spacing A°	Peak Intensity
1.	FOG-X-A	7.17	14.1	70
2.	FOG-X-B	7.86	13.5	121
3.	FOG-X-C	8.49	12.7	18.7
4.	FOG-D-A	7.34	13.4	120
5.	FOG-D-B	N/A	N/A	N/A
6.	FOG-D-C	N/A	N/A	N/A

3.9 FOG SEM Analysis

3.9.1 FOG-X-A and FOG-D-A

SEM analysis of framework of FOG-X-A and FOG-D-A at different magnification like (0.5 µm, 5 nm and 1 nm) as shown in the Figure 3.9.1, indicate that FOG-X-A have wrinkled curved morphology having look like stacked separated layers and mesoporous type structure similarly in FOG-D-A look like layered by layered structure having separated layers, cross-linked type as shown in figure 3.9.1 [10, 15, 16] .

3.10 FOG TGA Analysis

3.10.1 FOG-X-A and FOG-D-A

Thermal stability of framework FOG-X-A and FOG-D-A have been measured through thermal gravimetric analyzer shows that FOG-X-A loss 24 % weight loss up to 100 °C due to absorbed moisture , 30 % weight loss up to 200 °C due to the removal of less stable molecules while 41 % weight loss up to 300 °C due to removal of more stable molecules in framework. Similarly for FOG-D-A 12 % weight loss up to 100 °C is due to loss of moisture and 51 % weight loss is due to less stable molecules on the surface of framework while 57 % weight loss up to 200 °C is due to removal of more stable groups as compared to both FOG-X-A is more stable as compared to FOG-D-A [10, 17].

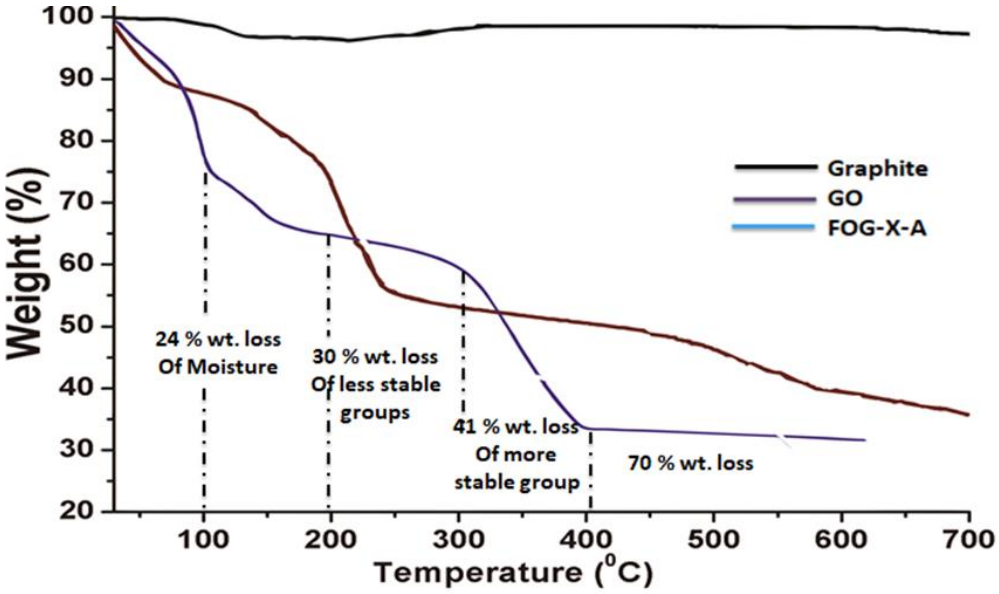

Figure 3.10.1 TGA of FOG-X-A

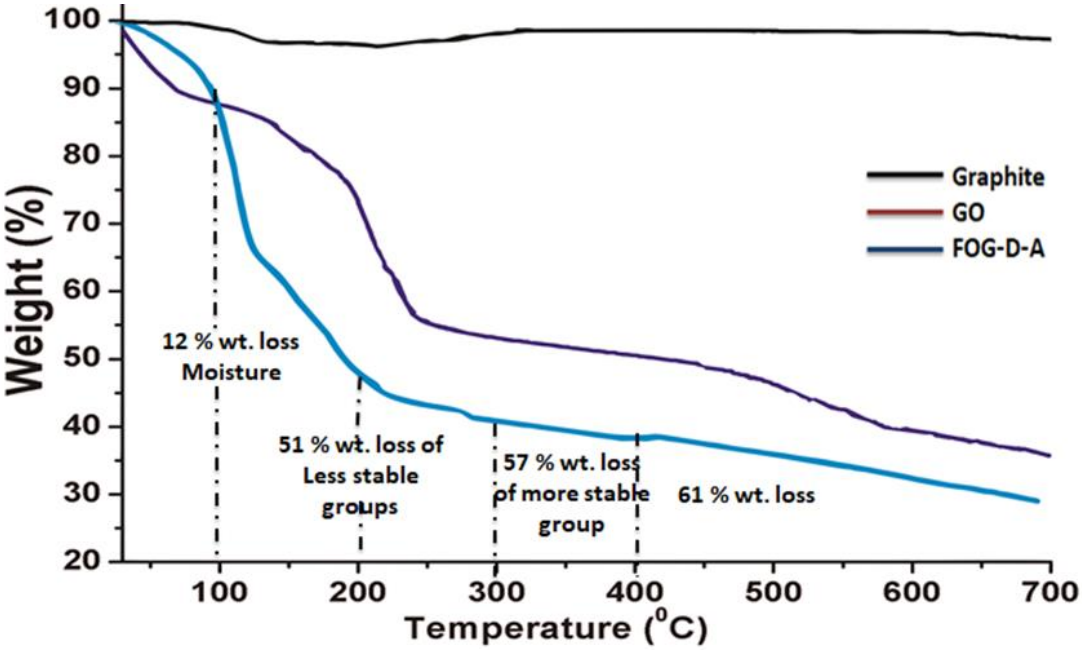

Figure 3.11.1 TGA of FOG-D-A

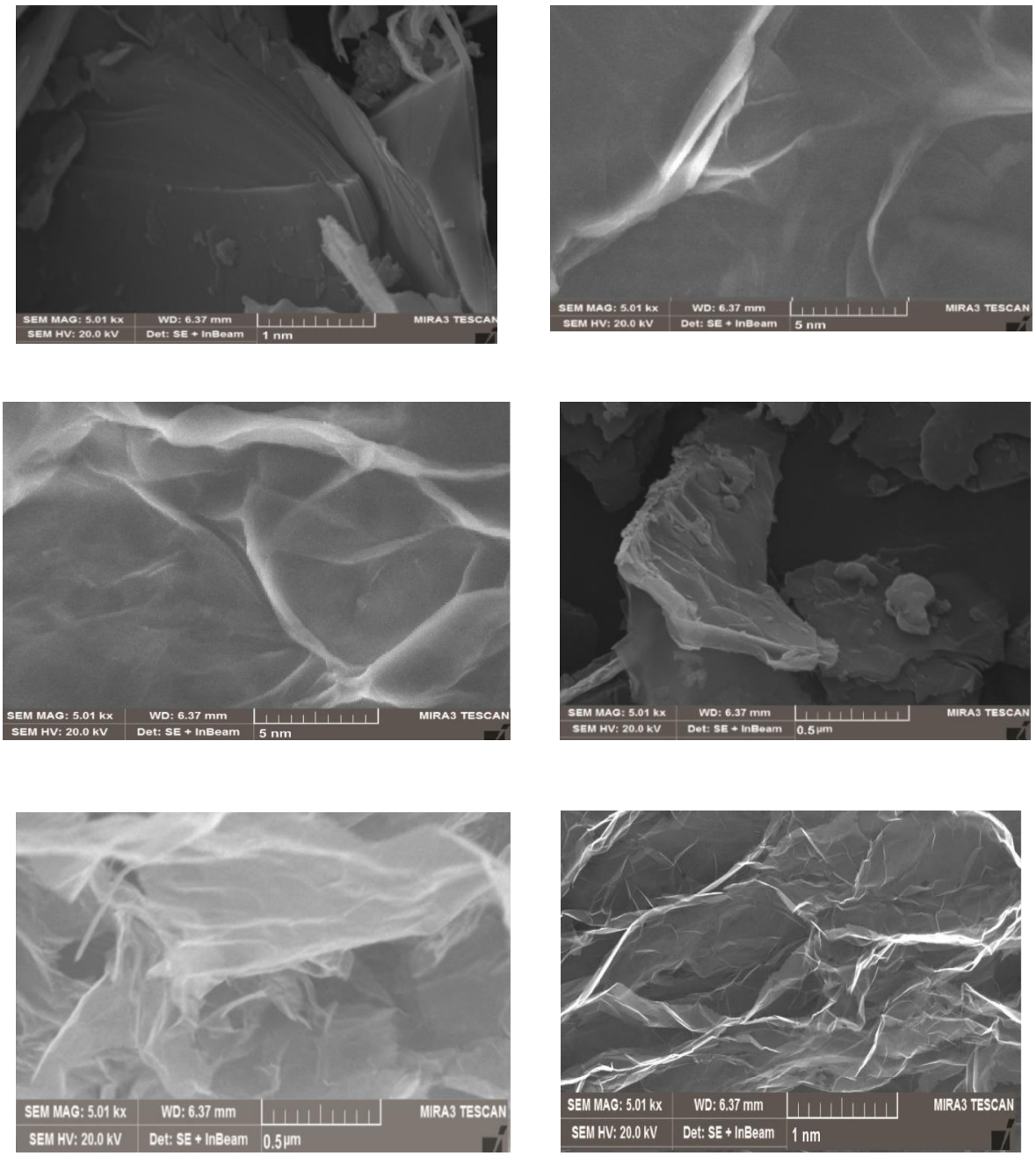

Figure 3.9.1 SEM of FOG-X-A and FOG-D-A

3.11 FOG BET Analysis

3.11.1 GO, FOG-X-A and FOG-D-A

Surface area of sample was measured by Brunauer-Emmett-Teller instrument was measured at 77 K using N2 as an adsorption gas. The measured surface area of GO, FOG-X-A and FOG-D-A, surface area enhance from GO to linker due to more spacing between the layers of GO are given in Table 4.5 [9, 16, 18].

Table 3.11.1 BET Surface area of GO, FOG-X-A and FOG-D-A

Samples	Surface area (m^2/g)
GO	52
FOG-X-A	392
FOG-D-A	284

3.12 Electrochemical performance

In order to examine the performance of as-fabricated graphene materials for supercapacitor application, three electrode system was used using FOG X-A, FOG X-B, FOG X-C, FOG D-A, FOG D-B and FOG D-C as working electrode materials, respectively, with Ag/AgCl as a reference electrode and a platinum (Pt) as counter electrode. The measurements were carried out at the ambient temperature using 1 M H_2SO_4 aqueous electrolyte. Electrochemical tests such as cyclic voltammetry (CV), galvanostatic charge discharge and electrochemical impedance spectroscopy (EIS) were performed.

3.12.1 Cyclic Voltammetry Curves (CV)

CV was done for all synthesized samples from 0.2 to 0.8 at different scan rates i-e 10 mVs^{-1}, 50 mVs^{-1} and 100mVs^{-1}. The curves indicate the oxidation and reduction behaviour of the samples used and the prominent faradic redox peaks can be observed in Figure 3.12.1. The peaks show the pseudocapacitive behaviour. FOG X-A exhibits the highest redox peaks at any scan rate which is ascribed to the redox behaviour of the intercalated amine groups. By

increasing the scan rate, the quasi-symmetric redox peaks and the analogous CV curve shapes are witnessed, proposing the ideal pseudocapacitive performance and the rate proficiencies or capabilities of the fabricated electrode materials [19, 20]. Furthermore, on increasing scan rate the cathodic peaks shifts towards the lower potential while the anodic peaks move to higher potential because of the insufficient of the ions from electrolyte to the graphene layers. At the same time, the cathodic current density decreases and increase in the anodic current density occurs which is the indicative of low resistance and rapid redox reaction at the electrode/electrolyte interface. The specific capacitance values are calculated by using formula shown in equation (3.1)

$$\mathbf{Csp} = \frac{\mathbf{1}}{\boldsymbol{s \cdot m \cdot V}} \int_{\boldsymbol{v1}}^{\boldsymbol{v2}} \boldsymbol{i \delta V} \qquad \textbf{Eq 3.1}$$

Where,

C_{sp}: specific capacitance **(F g^{-1})**

s: scan rate **(V s^{-1})**

m: mass of active material **(g)**

V: voltage difference **(Volt)**

i: current **(Amp)**

V1: lower voltage limit **(Volt)**

V2: upper voltage limit **(Volt)**

The specific capacitance for all samples shown in Table 3.12.1 indicates that the sample FOG X-A has the highest **C_{sp}** value i-e 360Fg^{-1} at 20mVs^{-1} whereas the lowest value is observed for the FOG D-C i-e 29.37 Fg^{-1} at 20mVs^{-1}. Figure 3.12.1.1 is the descriptive picture of the results indicates the maximum specific capacitance value for the FOG X-A.

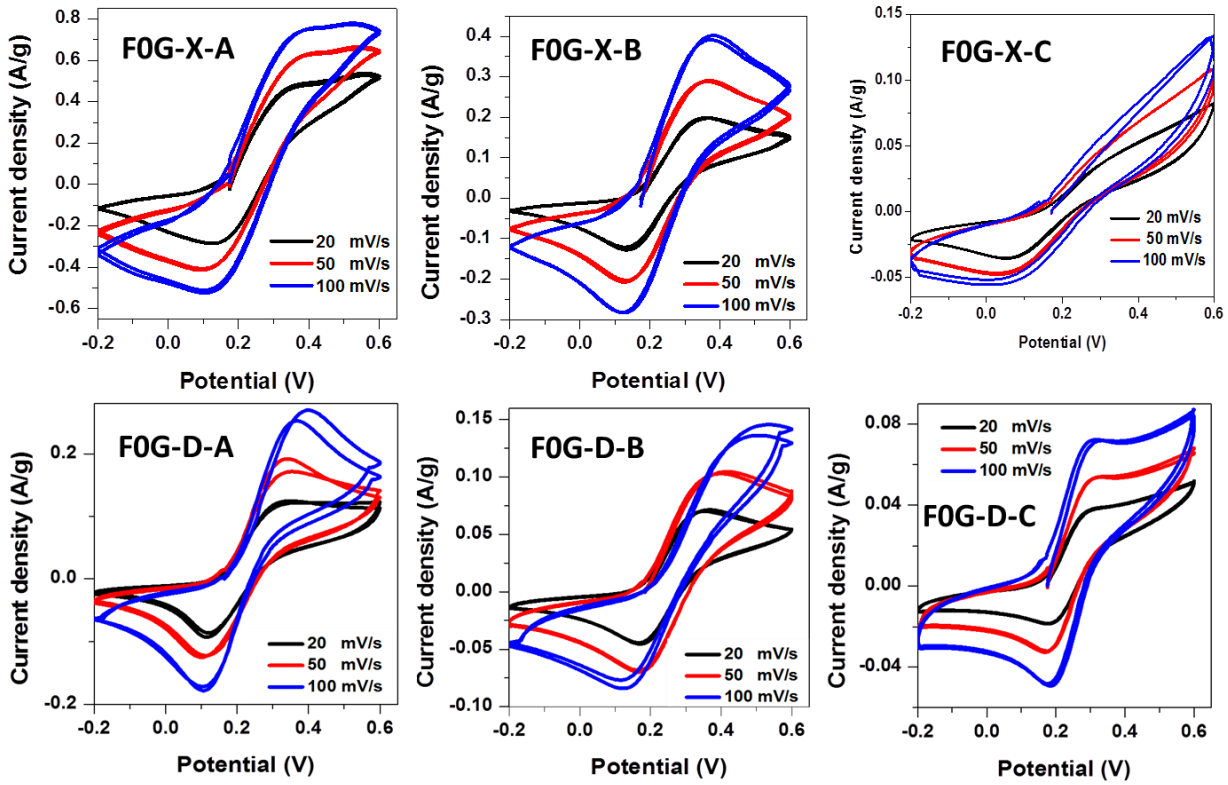

Figure 3.12.1. CV curves (a) FOG-X-A (b) FOG-X-B (c) FOG-X-C (d) FOG-D-A (e) FOG-D-B (f) FOG-D-C

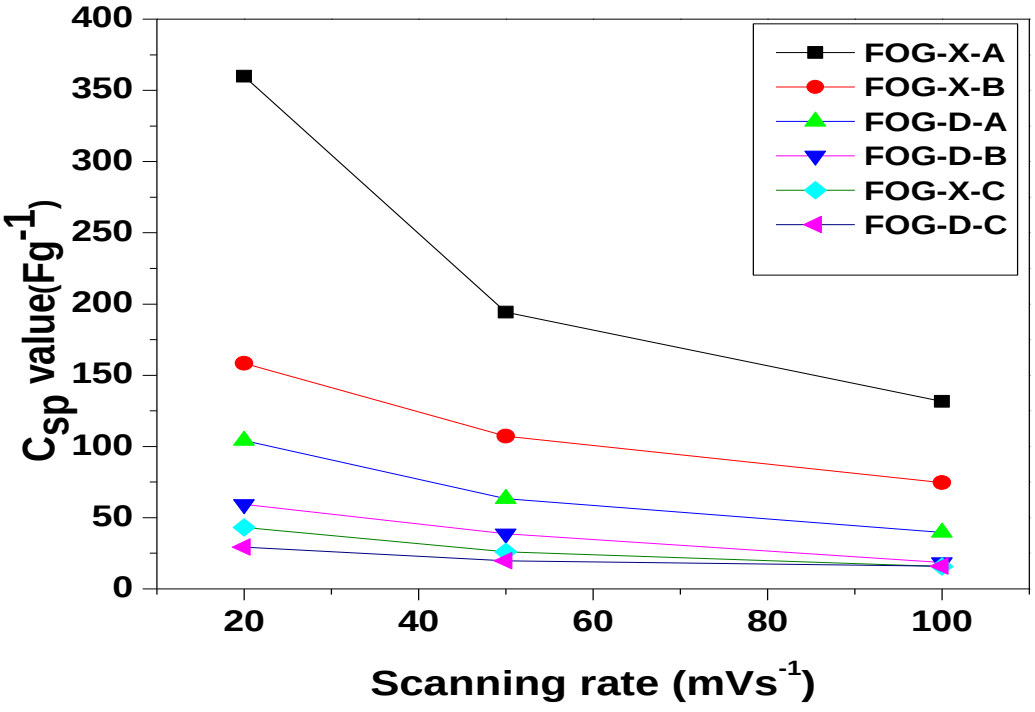

Figure3.12.1.1: Specific capacitance values for all samples at scanning rates 20 mVs^{-1}, 50 mVs^{-1} and 100 mVs^{-1}

Table 3.12.1 Specific capacitance values for all samples at scanning rates 20 mVs-1, 50 mVs-1 and 100 mVs-1

Scanning rate (mVs^{-1})	C_{sp} value (Fg^{-1}) FOG-X-A	C_{sp} value (Fg^{-1}) FOG-X-B	C_{sp} value (Fg^{-1}) FOG-X-C	C_{sp} value (Fg^{-1}) FOG-D-A	C_{sp} value (Fg^{-1}) FOG-D-B	C_{sp} value (Fg^{-1}) FOG-D-C
20	360	158.25	43.06	104.2	59.35	29.37
50	194	107.29	25.95	63.87	38.70	19.74
100	131.62	64.65	15.78	39.66	18.63	15.85

3.12.2 The galvanostatic charge–discharge curves

The galvanostatic charge–discharge is the complimentary technique to justify the above results. The charging discharging curves observed in Fig 3.12.2 for all the synthesized samples are non- symmetric [21]. This behaviour attributes to the pseudocapacitive nature of the materials. If we focus on the curves we can see that the small potential drop or IR drop is observed for the FOG X-A and the largest for the FOG D-C. IR drop is the sudden potential drop due to the internal electrode resistance, greater the potential drop lesser will be the efficiency of the electrode material and smaller will be the specific capacitance. This shows that FOG X-A is the best material for the supercapacitor with least potential drop.

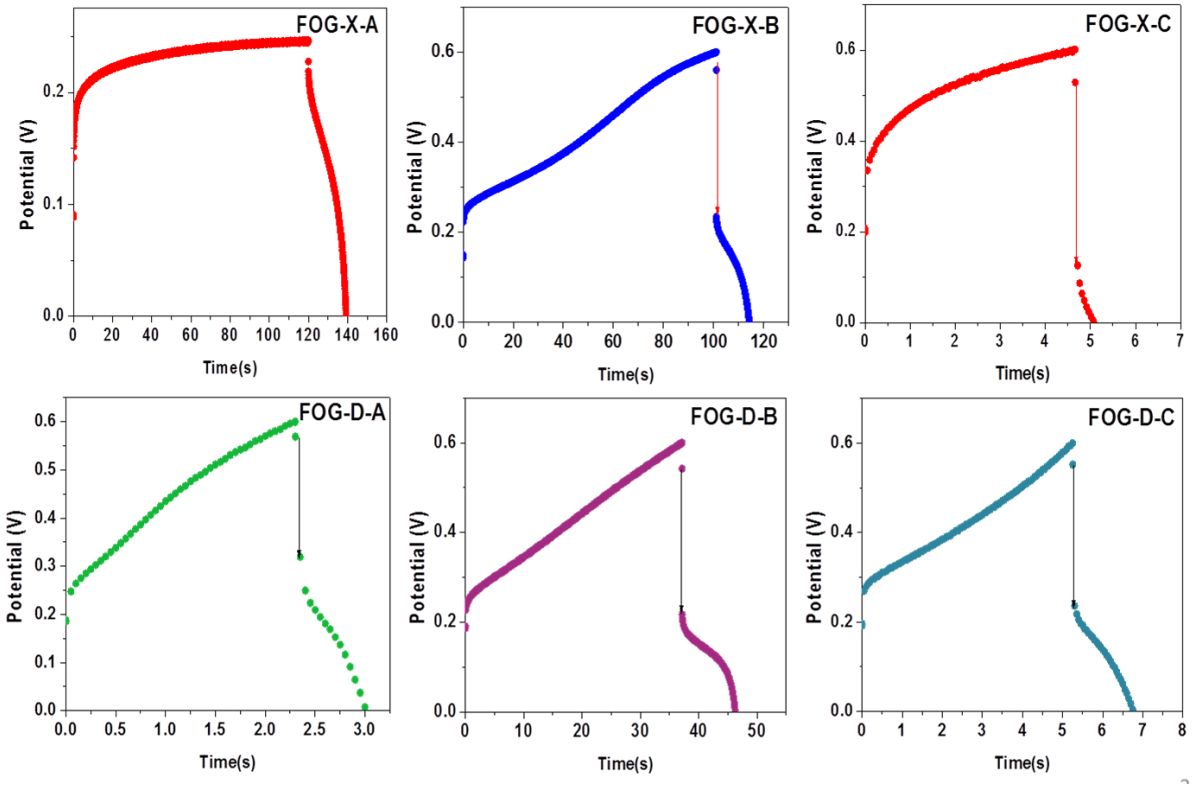

Figure 3.12.2 Galvanostatic charge-discharge curves for all samples.

3.12.3 Electrochemical impedance spectroscopy (EIS)

Electrochemical impedance spectroscopy (EIS) was used to examine the charge transfer behaviour in GOF (graphene oxide frameworks) based electrodes. Figure 3.12.3 illustrates the Nyquist plot of fabricated modified graphene materials based electrodes, which we have recorded at 0.4V in the frequency range of 100 kHz to 0.01Hz. The Nyquist plot comprises of tiny semi-circular part in the high frequency region and almost vertical line in the low frequency region. As in high frequency region a semi-circular arc is observed in the plots of all samples which is associated with the electron transfer mechanism at the interface between the electrolyte and electrode. It is clear from the plot that FOG X-A shows smallest semi-circle in high frequency region while FOG D-C shows largest semi-circle at large frequency. So it is indicative of the small charge transfer resistance in case of earlier FOG X-A as compared to the FOG D-C. The larger semicircle for FOG D-A suggests that it has a higher charge transfer resistance because of the restacking and aggregation in the reduction process. The straight line of the plot which is connected to the semicircular region shown in Figure 3.12.3. is the indicative of Warburg impedance (WI) that is the measure of the resistance to the diffusion of the electrolyte in the system [22, 23]. It is evident that in case of FOG X-A

the slop is linear close to x-axis; the WI is minimum which means it facilitates the diffusion of electrolyte due to having increased spacing between the layers. Whereas, WI is maximum in case of FOG D-C due to very large linear part which reveals that it has large resistance to the electrolyte diffusion. These results support the higher specific capacitance value observed for the FOG X-A (Table 3.12.1). This impedance study clearly demonstrates and validates the previous results in terms of charge kinetics.

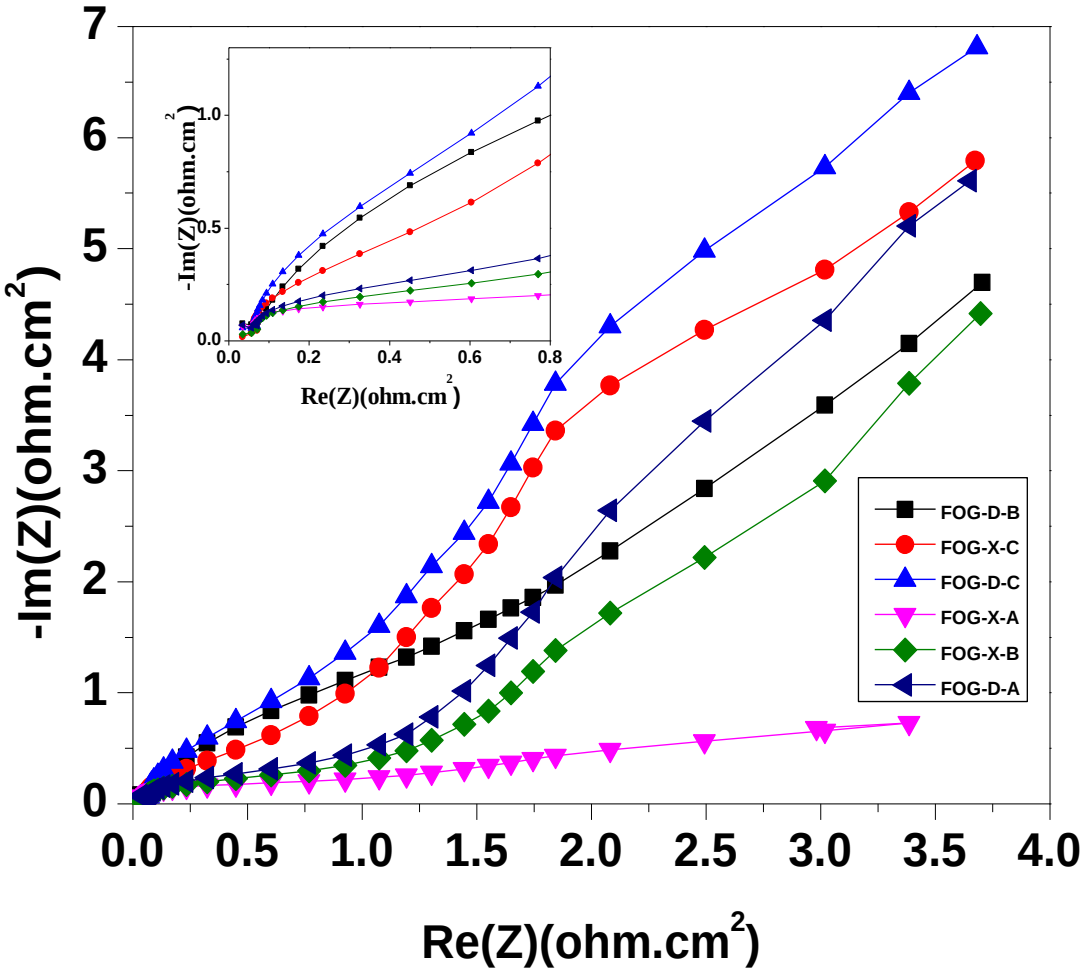

Figure 3.12.3: Nyquist plots of as-synthesized materials based electrode of all samples.

3.13 Formation mechanism of graphene oxide

The active species to oxidize graphite is diamanganese heptoxide (Mn_2O_7) which is obtained via the reaction of monometallic tetra oxide and MnO^{3+} [24] as shown in the reaction below [25].

$$KMnO_4 + 3\,H_2SO_4 \longrightarrow K^+ + MnO_3^+ + H_3O^+ + 3\,HSO_4^- \quad \text{Eq 3.2}$$

$$MnO_3^+ + MnO_4^- \longrightarrow Mn_2O_7 \quad \text{Eq 3.3}$$

The transformation of MnO_4 into a more reactive form Mn_2O_7 will certainly help oxidize graphite powder as shown in the reaction below [26]

$$Mn_2O_7 + H_2SO_4 + C(\text{graphite}) \longrightarrow \begin{matrix} C\ O\ C \\ C\ OH \\ COOH \end{matrix} + MnO_5 + H_2O + SO_2 \quad \text{Eq 3.4}$$

But the bimetallic form of manganese oxide has been reported to detonate when heated up to 55°C temperature or when reacted with organic compounds [27].

3.14 Proposed Mechanism of synthesis of FOG using 1,4-XDA and 2,6-DAP

Graphene oxide has numerous oxygenated groups such as hydroxyl, epoxy and carboxylic groups. These functional species offer the probability of covalently grafting the active molecules onto graphene sheets [28]. In our study, 1,4-XDA and 2,6-DAP were adopted to functionalize GO using the oil bathing process. It has been proposed that the modification of GO is achieved by epoxy ring-opening reaction [29] between the amine groups of 1,4-XDA or 2,6-DAP and the epoxy groups on the GO basal plane (Scheme 1). However the carboxyl groups on the edges might react with 1,4-XDA or 2,6-DAP through amide linkage shown in (Scheme 2 and 3). FOG was synthesized through 'Reaction first then Reduction' process. 1,4-XDA or 2,6-DAP molecules were inserted into the space of graphene sheets and prevent them from restacking[23].

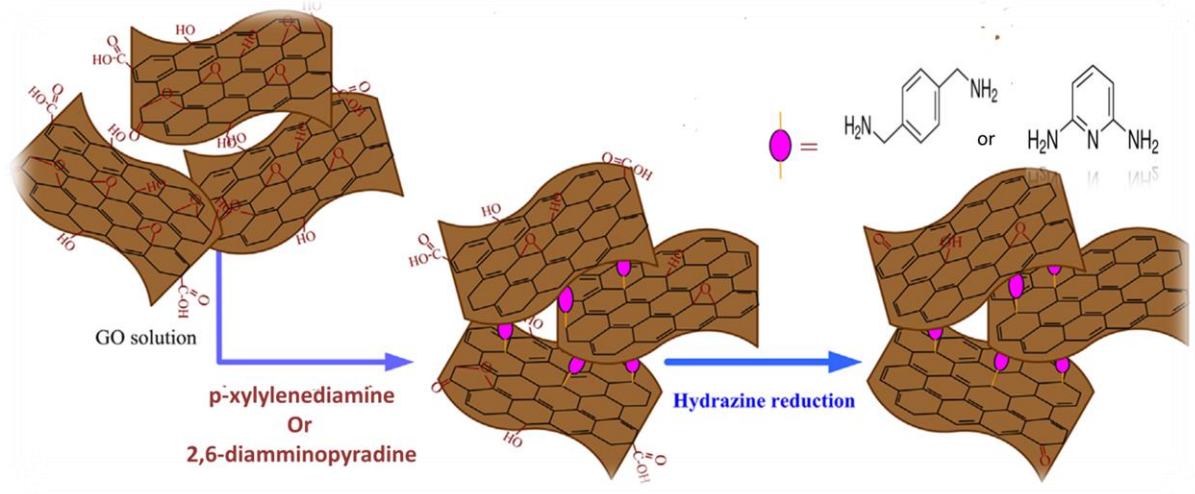

Scheme 1: Synthesis of the FOG using 1,4-XDA or 2,6-DAP via epoxy ring opening reaction

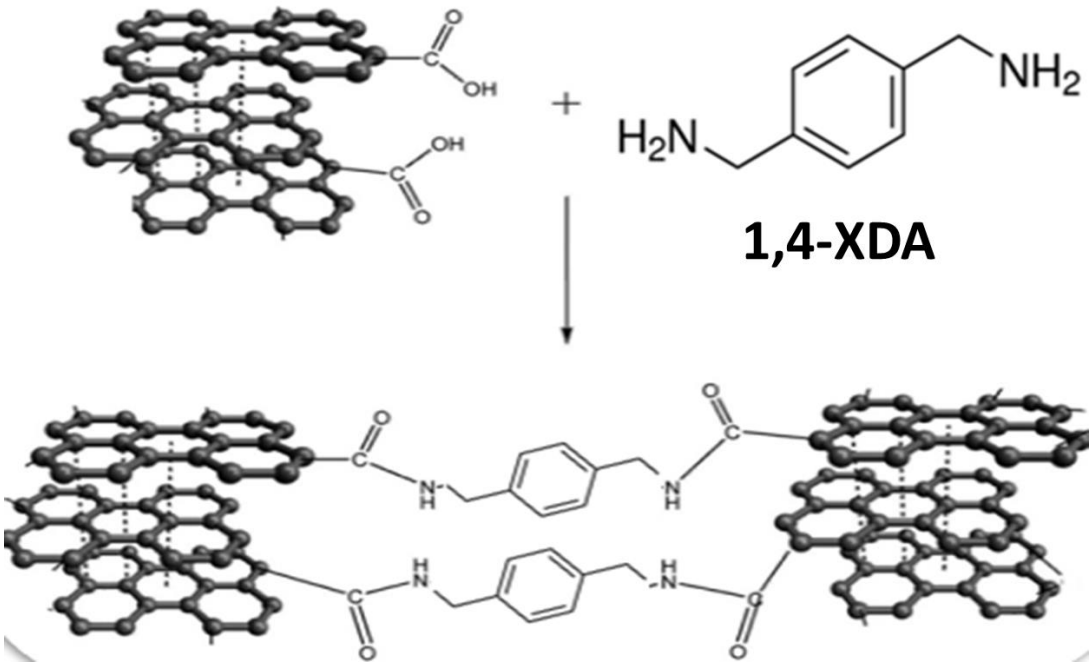

Scheme 2: Synthesis of the FOG using 1,4-XDA via amide linkage

Scheme 3: Synthesis of the FOG using 2,6-DAP via amide linkage

Conclusion

Highly exfoliated and more oxidized graphene oxide sheets obtained by Improved Hummer's method. Framework of graphene oxide (FOG) obtained by reflux reaction with three different ratio of GO: Linker molecules of 1,4-XDA and 2,6-DAP have successfully utilized to produce framework. Characterization of the synthesized materials through (FTIR, XRPD, TGA & SEM) proved that the successful synthesis of (FOG) materials. BET surface area enhanced from graphene oxide (52 m^2/g) to (FOG) materials (392 m^2/g) give route for supercapacitance application, so we hope that our material is good in the query of supercapacitance. Electrochemical performance of all synthesized materials has been observed through Cyclic voltammetry, Galvanostatic charge discharge and Electrochemical impedance spectroscopy. Among the all synthesized samples FOG-X-A is proved to be the best material for supercapacitors with C_{sp} value of 360 Fg^{-1}.

Reference

[1] D. R. Dreyer, S. Park, C. W. Bielawski, and R. S. Ruoff, "The chemistry of graphene oxide," *Chemical Society Reviews,* vol. 39, pp. 228-240, 2010.

[2] P. B. Arthi G and L. Bd, "A Simple Approach to Stepwise Synthesis of Graphene Oxide Nanomaterial," *Journal of Nanomedicine & Nanotechnology,* vol. 06, 2015.

[3] J. Chen, B. Yao, C. Li, and G. Shi, "An improved Hummers method for eco-friendly synthesis of graphene oxide," *Carbon,* vol. 64, pp. 225-229, 2013.

[4] H. Imran, P. N. Manikandan, and V. Dharuman, "Facile and green synthesis of graphene oxide by electrical exfoliation of pencil graphite and gold nanoparticle for non-enzymatic simultaneous sensing of ascorbic acid, dopamine and uric acid," *Rsc Advances,* vol. 5, pp. 63513-63520, 2015.

[5] H. Feng, R. Cheng, X. Zhao, X. Duan, and J. Li, "A low-temperature method to produce highly reduced graphene oxide," *Nature Communications,* vol. 4, p. 1539, 2013.

[6] A. Hussein, S. Sarkar, D. Oh, K. Lee, and B. Kim, "Epoxy/p-phenylenediamine functionalized graphene oxide composites and evaluation of their fracture toughness and tensile properties," *Journal of Applied Polymer Science,* vol. 133, 2016.

[7] R. Kumar, S. Naqvi, N. Gupta, K. Gaurav, S. Khan and P. Kumar, "Bulk synthesis of highly conducting graphene oxide with long range ordering," *RSC Adv.,* vol. 5, pp. 35893-35898, 2015.

[8] Z.-z. Yang, Q.-b. Zheng, H.-x. Qiu, J. Li, and J.-h. Yang, "A simple method for the reduction of graphene oxide by sodium borohydride with CaCl2 as a catalyst," *New Carbon Materials,* vol. 30, pp. 41-47, 2015.

[9] J. W. Burress, S. Gadipelli, J. Ford, J. M. Simmons, W. Zhou, and T. Yildirim, "Graphene oxide framework materials: theoretical predictions and experimental results," *Angewandte Chemie International Edition,* vol. 49, pp. 8902-8904, 2010.

[10] X. Lu, L. Li, B. Song, K.-s. Moon, N. Huand G. Liao, "Mechanistic investigation of the graphene functionalization using p -phenylenediamine and its application for supercapacitors," *Nano Energy,* vol. 17, pp. 160-170, 2015.

[11] L. N. Zhou, H. Zhao, Y. Liu, J. Li, H. F. Shi and Y. G. Wu, "Synthesis of Graphene Oxide Frameworks and their Application in Electrocatalytic Preparation of Hydrogen Peroxide," *Advanced Materials Research,* vol. 1090, pp. 43-49, 2015.

[12] R. Shah, A. Kausar, and B. Muhammad, "Characterization and Properties of Poly(methyl methacrylate)/Graphene, Poly(methyl methacrylate)/Graphene Oxide and Poly(methyl methacrylate)/p-Phenylenediamine-Graphene Oxide Nanocomposites," *Polymer-Plastics Technology and Engineering,* vol. 54, pp. 1334-1342, 2015.

[13] B. Feng, K. Xu, and A. Huang, "Covalent synthesis of three-dimensional graphene oxide framework (GOF) membrane for seawater desalination," *Desalination,* vol. 394, pp. 123-130, 2016.

[14] T. Tsoufis, G. Tuci, S. Caporali, D. Gournis, and G. Giambastiani, "p-Xylylenediamine intercalation of graphene oxide for the production of stitched nanostructures with a tailored interlayer spacing," *Carbon,* vol. 59, pp. 100-108, 2013.

[15] W.-S. Hung, C.-H. Tsou, M. De Guzman, Q.-F. An, Y.-L. Liu and Y.-M. Zhang, "Cross-Linking with Diamine Monomers To Prepare Composite Graphene Oxide-Framework Membranes with Varyingd-Spacing," *Chemistry of Materials,* vol. 26, pp. 2983-2990, 2014.

[16] R. Kumar, V. M. Suresh, T. K. Maji, and C. Rao, "Porous graphene frameworks pillared by organic linkers with tunable surface area and gas storage properties," *Chemical Communications,* vol. 50, pp. 2015-2017, 2014.

[17] H.-L. Ma, H.-B. Zhang, Q.-H. Hu, W.-J. Li, Z.-G. Jiang and Z.-Z. Yu, "Functionalization and Reduction of Graphene Oxide withp-Phenylene Diamine for Electrically Conductive and Thermally Stable Polystyrene Composites," *ACS Applied Materials & Interfaces,* vol. 4, pp. 1948-1953, 2012.

[18] L. T. Hoa and S. H. Hur, "Non-Enzymatic Glucose Sensor Based on 3D Graphene Oxide Hydrogel Crosslinked by Various Diamines," *Journal of Nanoscience and Nanotechnology,* vol. 15, pp. 8697-8700, 2015.

[19] Y. You, H. R. Yao, S. Xin, Y. X. Yin, T. T. Zuo and C. P. Yang, "Subzero-Temperature Cathode for a Sodium-Ion Battery," *Advanced materials,* vol. 28, pp. 7243-7248, 2016.

[20] F. Lu, M. Zhou, W. Li, Q. Weng, C. Li and Y. Xue, "Engineering sulfur vacancies and impurities in NiCo2S4 nanostructures toward optimal supercapacitive performance," *Nano Energy,* vol. 26, pp. 313-323, 2016.

[21] W. He, C. Wang, H. Li, X. Deng, X. Xu, and T. Zhai, "Ultrathin and Porous Ni3S2/CoNi2S4 3D-Network Structure for Superhigh Energy Density Asymmetric Supercapacitors," *Advanced Energy Materials,* vol. 7, p. 1700983, 2017.

[22] Y. Wang, Z. Shi, Y. Huang, Y. Ma, C. Wang and M. Chen, "Supercapacitor devices based on graphene materials," *The Journal of Physical Chemistry C,* vol. 113, pp. 13103-13107, 2009.

[23] X. Lu, L. Li, B. Song, K.-s. Moon, N. Hu and G. Liao, "Mechanistic investigation of the graphene functionalization using p-phenylenediamine and its application for supercapacitors," *Nano Energy,* vol. 17, pp. 160-170, 2015.

[24] A. M. Dimiev and J. M. Tour, "Mechanism of graphene oxide formation," *ACS nano,* vol. 8, pp. 3060-3068, 2014.

[25] K. R. Koch, "Oxidation by Mn207: An impressive demonstration of the powerful oxidizing property of dimanganeseheptoxide," *Journal of Chemical Education,* vol. 59, p. 973, 1982.

[26] A. Allahbakhsh, F. Sharif, S. Mazinani, and M. Kalaee, "Synthesis and characterization of graphene oxide in suspension and powder forms by chemical exfoliation method," *International Journal of Nano Dimension,* vol. 5, pp. 11-20, 2014.

[27] T. F. Emiru and D. W. Ayele, "Controlled synthesis, characterization and reduction of graphene oxide: A convenient method for large scale production," *Egyptian Journal of Basic and Applied Sciences,* vol. 4, pp. 74-79, 2017.

[28] A. B. Bourlinos, D. Gournis, D. Petridis, T. Szabó, A. Szeri, and I. Dékány, "Graphite oxide: chemical reduction to graphite and surface modification with primary aliphatic amines and amino acids," *Langmuir,* vol. 19, pp. 6050-6055, 2003.

[29] Q. Wu, Y. Sun, H. Bai, and G. Shi, "High-performance supercapacitor electrodes based on graphene hydrogels modified with 2-aminoanthraquinone moieties," *Physical Chemistry Chemical Physics,* vol. 13, pp. 11193-11198, 2011.

Zohaib

by Hafiz Muhammad Zohaib

FILE	PLAGRISM_REPORT_2.DOCX (74.27K)		
TIME SUBMITTED	31-AUG-2018 09:44AM (UTC+0500)	WORD COUNT	6368
SUBMISSION ID	995280964	CHARACTER COUNT	34386

The name graphite carbon is derived from the Latin word "carbo" meaning charcoal. This element is distinctive and form well-known stable allotropes as its electronic structure allows for sp, $sp^2$and sp^3 hybridization networks. Graphite an abundant natural mineral is the most common crystalline allotropic form of carbon and has been known ever since antiquity together with diamond. Graphite has a planar, layered structure consists of atomic layers of sp^2 hybridized carbon atoms stacked together via van der Waals force. The carbon atoms in every layer are arranged in honey comb like lattice with 0.142 nm separation and d-spacing between planes is 0.34 nm. All atoms in plane are covalently bonded; merely three of the four bonding sites are satisfied however the fourth electron is allowed freely to move in the plane making graphite electrically conductive in the direction parallel to the plane. Though the vast delocalized electrons are available in between the layer so at right angle to the plane it is non-conductive in nature(1).

The individual layer of sp^2 hybridized carbon atoms firmly packed into a two-dimensional (2D) hexagonal honeycomb like crystal lattice is called graphene(2). This name was first introduced by Stumpp, Setton and Boehm, in 1994(3). It acts as the basic building block for graphitic derivatives of all other dimensionalities, such as fullerenes (0D), carbon nanotubes (1D) and graphite (3D) (4). Graphene is a semi-metal with zero bandgap due to slight overlap between the valence and the conduction bands (zero bandgap material). In the graphene layer each carbon atom form three sigma bonds by overlapping of sp^2 orbitals with neighboring carbon atoms whereas the band of filled π-orbital(valance band) and empty π* orbitals (conduction band) is formed by the overlapping of the remaining p_z orbitals which are accountable for the high in-plane electrical and thermal conductivity.

Graphene has the exceptional outstanding properties including high electron mobility i-e upto 200,000 $cm^2V^{-1}s^{-1}$ (5), high mechanical strength i-e Young's modulus ~1 T Pa (6), outstanding thermal conductivity i-e 5000$Wm^{-1}K^{-1}$], 97.7% optical transparency (7) and large specific surface area approximately 2630 m^2g^{-1} hence, it has drawn marvelous attention from researchers. Graphene -based sheets have been used in high performance catalysis (8), nanocomposites (9), high performance energy storage devices (10), chemical and biological sensors (11), optoelectronics and electronics (12) etc.

Graphite oxide has a stacked or layered structure like graphite, but in graphite oxide graphitic carbon is well decorated by oxygenated functionalities, which not only make the graphite oxide hydrophilic in nature but also enhance its inter-layer spacing. These oxidized graphite oxide layers can exfoliate in water or other solvents under ultrasonication. If the highly exfoliated sheets like graphene have one or few carbon atom layers, then these are named as graphene oxide (GO). GO has a mono atomic layered structure composed of carbon, oxygen and hydrogen molecules synthesized by the oxidation of inexpensive and abundantly existed graphite crystals. Due to its hydrophilic character it can disperse in

water more easily than other solvents and convenient to process. Most importantly the Graphene oxide can be reduced partially by the reduction of oxygenated groups to graphene sheets. The chemically derived GO have given many other names as functionalized graphene oxide, frame works of graphene, reduced graphene or chemically modified graphene.

i. Graphene oxide (GO) have two significant features: GO can be synthesized or produced with high yield via cost effective chemical route using cheap graphite as a raw material.

ii. As GO is hydrophilic in nature it can form highly stable aqueous colloids to aid the formation of macroscopic structures by inexpensive and simple solution process.

The graphene sheets comprise of trigonally bonded sp^2 hybridized carbon atoms and apart from micro-ripples it's completely flat. However, GO sheets partly compose of tetrahedral bonded sp^3 hybridized carbon atoms, which are slightly displaced below or above the graphene plane. Because of the existence of covalently bonded functional moieties and structural deformation, the sheets of graphene oxide are atomically rough. Several researchers have investigated and observed that the surface of graphene oxide has defective regions because of the presence of oxygen and the other areas are almost intact. According to a report honey comb like lattice structure remain preserved in GO as like graphene however, slight displacement of carbon atoms due to attached functional groups but the size of the unit cell remains the same as that of graphene. Hence forth GO can be defined as irregular oxidized oxygen containing regions along with non-oxidized areas having sp^2 hybridized carbon atoms.

As the interplanar distance (d-spacing) between the stacked layers of the graphite valued to be 0.34 nm and is not adequate to host inorganic and organic ions/molecules or other species. However in order to enhance the graphite interlayers spacing from 0.335nm to higher values numerous intercalation approaches have been applied, depending on the size of the guest species. Ever since the intercalation of graphite with potassium, a series of chemical species have been tried to make what we called graphite intercalation compounds (GICs). These compounds could be formed by the insertion of intercalated species between the graphene layers via polar or ionic associations without altering the graphene structure. GICs can be synthesized not only with alkali metals (like sodium, potassium, lithium etc.) but also with anionic species like bisulfate, nitrate, or halogens.

In other type of case the inserted molecules may interact with covalent bonding through chemical grafting reactions within the graphite interlayer spacing; this results in the structural changes of the graphene planes as the hybridization changes from sp^2 to sp^3 of the reacting graphitic carbon atoms. A characteristic example of GICs is the reaction of graphite with strong acids and oxidizing agents that generates oxygen

functional groups not only on the surfaces but also at the edges of the graphene layers results into the formation of graphite oxide.

First, in 1840 Schafheutl(13) and after 19 years in 1859 Brodie (14)were the pioneers in the formation of graphite oxide. The earlier fabricated graphite oxide with a mixture of nitric and sulfuric acid, while the later treated fuming nitric acid and potassium chlorate with raw graphite material. Staudenmaier (15)modified the Brodie method where oxidation of the graphite was done by the addition of concentrated H_2SO_4 and HNO_3 with potassium chlorate. After a century Hummers and Offeman(16) in 1958, reported that by immersing graphite in a mixture of $NaNO_3$, H_2SO_4, and KMnO4 oxidation occurs by the reaction of intercalated anions with carbon atoms of the graphitic layers resulted into the loss of the aromatic character. The robust oxidative reaction of these species with graphite leads to the generation of anionic groups mostly carboxylates, hydroxylates and epoxy groups on the surface and edges of the graphitic layers. The out of plane covalent bonds (like C–O) enhance the spacing between the graphene layers from 0.34 nm in graphite to around 0.68 nm(17) in graphite oxide. This newly developed polar or anionic character and enhanced inter spacing due to oxygen containing groups makes GO strongly hydrophilic in nature, which permits water molecules to penetrate within the graphene sheets thus forced the layers to further move apart. Thus graphite oxide can more easily in water than any other solvent. During the formation of graphite oxide the hybridization of carbon atoms changed from sp^2 to sp^3 which results into the disruption of the delocalized π system and thus electrical conductivity deteriorates between 103 to 107 Ω cm according to the quantity of oxygen(1, 18).

To inhibit the agglomeration of the GO sheets and to enhance the performance of graphene-based semiconductors (19) numerous methods have been introduced (20, 21). These methods modify graphene properties by introducing covalently or non-covalently dopants or fillers to GO sheets (22, 23). For example, conducting polymers (24), carbon nanotubes (25, 26), heteroatoms (24) and transition metal oxides (27)were studied and adopted for Graphene oxide (GO) surface modifications, which would inhibits the aggregation or restacking of graphene layers or sheets and they may server as the spacers or may add redox active functional species that would enhance the capacitance of GO. However, some disadvantages have been associated with non-covalent approaches, like the molecules may slip pass over each other, and they are unstable and difficult to control in contrast to the covalent approaches (28). Therefore, for this purpose the covalent approaches are more promising way.

As reported in previously, phenylenediamine as a good molecule for the graphene oxide functionalization and it is quite effective to enhance the performance of the SCs (29, 30). It is well known that GO has large number of highly reactive functional groups on its surface, which allows the grafting of small organic molecules covalently on GO layers/sheets by different reactions (31). The PPD (p-phenylenediamine) has

two amine groups (–NH2) on the benzene ring para-position that may react in certain conditions with the functional moieties present on the surface of GO layers, thus prevents the restacking or aggregation of the GO sheets by occupying the space between the graphene layers .Though, many researchers find out PPD as a good redox mediator and it accelerates the pseudocapacitance of SCs by rapid reversible faradaic reactions. Furthermore, PPD is also viewed as nitrogen doping precursor for the capacitance enhancement (32). Here, in our thesis we report the 1,4-XDA and 2,6-DAP modified GO composite materials by using the solution process. 1,4-XDA and 2,6-DAP functionalized GO composite materials have been used as the electrodes materials of SCs, exhibiting excellent electrochemical performance.

It is always remain challenging to produce Graphene oxide and modified graphene oxide materials in massive quantity and of high quality by using inexpensive, cheap and environmentally friendly methods

Mechanical exfoliation can be used for the production of the pristine graphene oxide but the drawback of this method is that its highly complicated and the small amount of product can be achieved which limits its large scale production.

CVD technique can also be used for the synthesis of graphene films with one or few layer thickness. The drawback of this process is that it requires elevated temperature upto1000C along with hydrogen as carrier gas and a flow of hydrocarbon precursor gas which limits or restricts its application range.

In this process pure graphene with excellent properties and perfect structure is synthesized. But it is not east to assemble the product in thin films due to its extremely small size. In addition to this, high energy is required during this process which restricts its application and use for large scale production

Chemical methods are one of the best method uses now days for the production of the pristine graphene and graphene modified materials. These methods include:

Graphene oxide (GO) was initially synthesized by Brodie in 1859 during his research work on graphite(33). The raw graphite was oxidized by adding potassium chlorate ($KClO_3$) to the mixture of graphite and nitric acid (HNO_3). The resulting light yellow color graphite oxide was obtained after repeatedly washing, filtration and drying and the product obtained is stable to further oxidation.

Staudenmaier modified the Brodie's work by mixing the graphite and nitric acid (HNO_3) mixture more acidic and followed by the gradual addition of $KClO_3$ to this mixture. These variations and modifications simplified the process and improved the GO quality. However the drawback of this method is it took long time for $KClO_3$ addition and as a by-product toxic gas chlorine dioxide is released.

The mixture of $KClO_3$ and HNO_3 was used earlier for the fabrication of nanotubes(34), fullerenes(35). However, the oxidation results into the production of many oxygen containing functional moieties such as lactose, ketones, carboxyl's and also discharge toxic gases dinitrogen tetraoxide (N_2O_4) and nitrogen dioxide (NO_2). That's why this method still needs modification.

Hummer and its coworkers developed a method for the synthesis of GO termed as Hummers method(16). In this process the water free mixture of $NaNO_3$, conc.H_2SO_4 and $KMnO_4$ was maintained for two hours below 45°C. The product obtained had a high degree oxidation as compared to the previously reported Staudenmaier method however in hummer's method it was found that the product has GO sheets along with some un-oxidized graphite. For the excellent complete oxidation of graphite pretreated hummers method was introduced by Kovtyukhova. He first added raw graphite material to the mixture of potassium persulfate ($K_2S_2O_8$), conc. H_2SO_4, and phosphorous pentaoxide (P_2O_5), this mixture was maintained at 80°C for several hours(36). This preoxidized product was then washed, filtered and dried in air. In 2010, Marcano *et.al* reported modified hummers method(37). In place of $NaNO_3$ they added phosphoric acid (H_3PO_4) and also increase the amount of potassium permanganate. This minimize the discharge of hazardous gases due to the removal of sodium nitrate thus prohibits the emission of N_2O_4, NO_2 and ClO_2. In improved hummers method(38) graphite is first mixed with conc. H_2SO_4 to form GIC and then followed by the gradual addition of $KMnO_4$ then deionized water is added followed by the addition of H_2O_2. The product is then washed with 30% HCl and deionized water and dried to obtain the GO.(Figure 1.6.4.2)

In brief summary, the improved hummers method have the potential for the mass production of GO without the discharge of any sludge or toxic gases.

Recent research indicates the implementation of the graphene based materials in various fields as it exhibit greater potential for different applications as chemical sensors (39), nanogeneratores (40), catalysts (41), solar cells (42), photocatalysts (43), hydrogen storage (44) and the most important supercapacitors.

Amongst these applications, GOF-based electrodes made-up for electrochemical performance by low cost and reliable methods have gained greater interest owing to their outstanding properties. For example, rGO sheets having large surface area with potential to substitute (ITO) indium tin oxide in light emitting diodes and touch screens, however mass production can be attained due to electrical conductivity and its transparency (45, 46). Furthermore, as compared to the rigid and indium tin oxide, rGO/rGOF is viable in processability and flexibility for assembly of electronic devices.

Supercapacitor, an electronic device also called ultracapacitors is a high quality capacitor and its capacitance occupy a niche in-between the batteries and simple capacitors. In simple way, we can say that supercapacitors store extra energy than simple capacitor however discharges more gradually, and it stores

less energy than battery but discharge that energy more quickly. This difference in the performance of supercapacitors originates from the most fundamental and important mechanisms of energy storage every technology, demonstrated in Figure 1.8.

In capacitors, two electrodes are separated by a superseding dielectric layer. When a potential is applied across the electrodes an equal and opposite charge develops on the both electrodes. However, when a device is powered it introduces a new current path between the two electrodes for the dissipation of charge and thus resultant current can be consumed. In contrast to the capacitors, batteries have two electrodes immersed in an ionically conducting electrolyte. A reversible chemical reaction takes place for the storage of energy on both electrodes. During charging, on one electrode oxidation takes place while on the other electrode reduction occurs however on discharging the reactions got reversed. Capacitor works on the principle of electrostatic charge storage without going through chemical reactions whereas batteries undergo chemical reactions to store energy at the two electrodes.

Supercapacitors utilize both the batteries and capacitors principle of energy storage. Supercapacitors like batteries have two electrodes and a conducting electrolyte however it stores energy via electrochemical reactions unlike batteries. Upon charging high charge density area develops near the interface by the migration of electrolyte mobile ions to the electrode surface. Nowadays, supercapacitor electrodes are synthesized with wide surface area, leading to more space for charging.

The energy storage in supercapacitors occurs at the electrode/electrolyte interface. Two different mechanisms operative in charge storage are:

- Electrostatic double-layer charging
- Faradaic charge transfer (pseudocapacitance)

Double-layer charging happens when we apply the potential difference across the two electrodes immersed in an ionically conducting electrolyte. The cations move towards one electrode and the anions migrates towards the other electrode. For ideally polarized electrodes, no charge transfer occurs at the electrolyte and electrode; however this phenomenon produces interfacial areas at both electrodes, where the positive and negative charges in the electrolyte balance charges at the both electrodes.

In contrast to the double layer capacitors pseudocapacitors store charge at the electrode surface via redox reaction. In an ideal double layer capacitor charge transfer doesn't occur at the interface but in case of pseudocapacitance charge transfer occurs in order to store energy.

For example, in case of ruthenium oxide (RuO_2) electrodes large amounts of charge have been stored through many electron-proton transfer reactions (47, 48). Reactions given in equation 1.1 and 1.2 have been proposed to describe the mechanism of charge storage.

During this reaction electrons are transferred as evident from eq.1.1; during charging process these electrons move via external circuit (which is attached to the counter electrode) and the current generated from the reverse reaction can be used to execute the electrical work.

This reversible process of charge storage via redox reactions is also named "Faradaic," as compared to the "non-Faradaic" process that regulates double-layer charging.

I. However carbon based electrode storage charges primarily by non-Faradic reactions but overall pseudocapacitance behaviour can be observed for energy storage by three main methods. Surface functionalization by introducing reactive species (typically nitrogen and oxygen)
II. Deposition of the electroactive polymers like polypyrrole and polyaniline.
III. Deposition of the elctroactive transition metal oxides like MnO_2, RuO_2 etc.

These methods can be used to enhance the overall capacitance up to many folds. As reported when polyaniline was deposited on carbon fibers the gravimetric capacitance increased from 30 Fg^{-1} to 150Fg^{-1}.

In order to characterize and illustrates the electrical performance of supercapacitors different techniques can be employed. The most important one we have used in our research is three electrode working system.

Before a comprehensive argument of electrochemical characterization methods, a comparison should be made amongst two and three electrode systems. As demonstrated in Figure 1.8.2.1, in two electrode measurement assembly which is composed of typically two symmetric electrodes it involves full device measurements. On the other side, in three electrodes working setup, the material needs to be analyzed is measured against the counter and the reference electrode. The counter electrode provides the current required to complete the circuit during measurements. It is usually inert n nature, such as Pt wire. The reference electrode is made up of material with a known oxidation reduction (redox) potential, e.g. the calomel electrode (Hg/Hg_2Cl_2) or $Ag/AgCl_2$ electrode. This reference electrode facilitates the accurate potential measurements at the working electrode. The two electrode working setup is usually used to characterize the entire made-up devices, whereas the three electrode working system is strategic for observing the important electrochemical properties of the working electrode material. The specific

capacitance values (in units of Fcm^{-3}, Fcm^{-2}, Fg^{-1}) measured from the two electrode system will be typically 4 times less than the three electrode system.

Cyclic voltammetry (CV) is a technique in which the potential (V) at the working electrode is swept back and forward at constant rate across a given potential window. The resultant current (I) produced is measured and then plotted against the potential (VA simple description of the potential (V) plotted against time (t) is illustrated in Figure 1.8.2.2(a).

In the case of ideal supercapacitor, the capacitance remains constant irrespective of the scan rate and it can be calculated the formula given by equation 1.2

For an ideal supercapacitor, the resultant current measured is plotted as shown in Figure 1.8.2.2 (b, c). When the voltage applied is positive, the resultant current must be positive and along negative voltage sweep the current should be negative constant. Typically, CV plots are presented as in Figure 2.3c, with the current (I) plotted verses the potential (V). In an ideal supercapacitor, the CV plot will be rectangular in shape (symmetric about the zero current axis) and it must follow Eq. 1.2. In reality supercapacitors don't typically exhibit such ideal behaviour but they do it under ideal condition of exceedingly low scan rate

Supercapacitors show non ideal or realistic behaviour at high scan rates. As shown in Figure the CV plot has specific leaf like shape due to extremely high scan rates, which leads to the rounding off of the corners of the CV plot.

This behavior originates from the rate-limiting phenomenon which includes electrolyte ion transport limitations and the limitations of electrical charge transport at the electrode. Because at extremely high scan rates due to transport limitations the interfacial double layer fails to form as it doesn't find much time.

Electrolyte degradation is another non-ideal behaviour observed in supercapacitor. All electrolytes have a restricted voltage stability window if its value exceeds beyond the limit it undergoes faradic reactions in the electrolyte. For example, potential window of ~ 1 V have been observed in aqueous electrolytes. Moreover, at extremely low or high potentials, water can be easily reduced or oxidized to form hydrogen and oxygen, respectively. These types of reactions, which lead to the transfer of charges across the interface of the electrode and electrolyte, add additional current to the system over that of the only double layer charging current. As shown in Figure 2.4 (b) *I* excess is the current that refers to the electrolyte degradation reactions and not to the charge storage, and while calculating the capacitance (using Eq. 1.2) it should be subtracted. Moreover, the electrolyte degradation can reduce the overall performance of the supercapacitor.

Unlike the current produced due to electrolyte degradation (*I* excess), pseudocapacitive current subsidize the energy storage competences of a device. Capacitive current produced at electrode surface due to faradic reversible reactions; enhance the capacitance due to double-layer charging. Figure 2.4 (c) displays the CV plot of pseudocapacitive system in which *I*Φ represents the capacitive current.

The capacitance of an electrode can be calculated by cyclic voltammetry however the galvanostatic charge/discharge technique is often preferred for this purpose(49). In this technique a constant charging current is applied until and unless a maximum potential is achieved, at that point discharge current of the same magnitude is applied to reach a minimum potential value. The potential (V) is observed as function of time (t). In CV constant voltage scan rate is used however galvanostatic charge/discharge curves use constant current and they may test more accurate performance.

Figure displays some characteristic galvanostatic charge/discharge plots. In an ideal supercapacitor (Figure 1.8.2.3 a) the galvanostatic charge and discharge curves must be symmetrical with throughout a constant slop. The formula given in Eq.1.3 can be used to calculate capacitance

The capacitance values calculated by using galvanostatic charge/discharge and CV give us the approximately similar values. However the only difference is that in former numerator is kept constant while denominator is kept constant shown in equation 1.2 and 1.3.

Liner plots are not usually observed in non-ideal conditions in supercapacitors. Such non-ideal behaviour can be observed in Figure 1.8.2.3 b due to exceeding electrolyte stability window. The decline in the slop of charge/discharge curves generally shows the charge transfer at the electrolyte/electrode interface. The reactions occur at the electrode and electrolyte give rise to the charge transfer and when the reactions takes place in the electrolyte it leads to its degradation with time and indicates that the reduction of potential window within the limits of the electrolyte stability window.

On the other hand reversible electrode reactions, could contribute to the charge storage pseudocapacitive behavior; however irreversible electrode reactions could leads to the degradation and it damage the electrode so it is undesirable.

Figure 1.8.2.3 c is the illustrations of another non-ideal behavior observed at very high current density for all supercapacitors. When the capacitor switches from charging to discharging an instantaneous drop in voltage can be measured. This drop in voltage, also term as the IR drop, originates due to the ohmic resistances in system. The ohmic resistances are the sum of electrolyte

resistance, electrode resistance, and any other resistance present in the system.

The third most commonly used technique to probe supercapacitor material is the Impedance spectroscopy. In this technique an alternating potential is applied over the wide range of frequencies and the phase shift and the amplitude of the resultant current is measured.

Figure represents the Nyquist plot that exhibits the typical behaviour of the supercapacitor comprising of a porous electrode. In case of ideal RC circuit, the Nyquist plot look like a vertical line at $Z' = R$. The term Z (omega) impedance consists of the both imaginary and the real part. By plotting the real part on the x-axis and imaginary part on the y-axis we will get the Nyquist plot. The semi-circular region in the plot is the characteristic of single RC-constant. Often only a small part of semicircular region becomes visible. A straight line at 45°C region is termed as the Warburg impedance. Whenever the diffusion effect dominates the electrochemical reaction process the impedance is termed as Warburg impedance. The Warburg impedance becomes small at high frequency as the diffusing reactants not need to move far. However at low frequency the Warburg impedance increases as the diffusing reactants have to move far.

Graphene Oxide (GO) have been synthesized by "Modified Hummers,, method" In which placed the beaker on ice-bath set temperature ≤ 5 °C, poured 140 ml conc.H_2SO_4 in it. Addition of 3 g of Graphite powder in to it with stirring until complete dispersion. Slowly Bit by bit addition of 9 g of $KMnO_4$ in the dispersion to kept temperature control ≤ 15 °C, for 6 hours. Addition of 140 ml distilled water slowly in it and control temperature below 90 °C. After stirring for 1 hour addition of 420 ml of distilled water in it with 30 ml of H_2O_2 and continue stirring overnight. Reaction mixture poured in falcon tube and centrifuge at 8000 rpm for 3 hours (2 times with water and one time with 5% HCl Washing) to separate the precipitated product. The obtained product was dried in vacuum oven for 24 hours at 60 °C, the dried product was 2.104 g (70.13%)

Graphene oxide dispersion prepared by dissolving 300 mg GO into 150 ml deionized water and sonicates it for 60 minutes. 300 mg Linker molecules (Para-Xylyenediamine and 2, 6-Diamino Pyridine) dissolved into 150 ml deionized water; pour this mixture into GO dispersion slowly by continuous stirring. The above dispersion sonicate for 60 minutes and placed in round bottom flask heating on oil bath at 80 °C with continuous stirring for 1 day. Addition of Hydrazine Hydrate (10 ml) to the above dispersion drop wise and shifted the dispersion for reflux at 90 °C for 12 hours. Mixture cooled at room temperature and washed with deionized water through flirtation assembly, the obtained product dried in vacuum oven at 60 °C for 24 hours [3, 4]. Similarly as above three different concentration of GO: Linker dispersion ratios have been prepared.

Atomic vibration in molecules provides information about functional groups in material that was obtained through FTIR techniques. In figure 4.1.1 show the FTIR spectra of graphite powder that is featureless, no functional groups present in graphite, while in figure 4.1.2 the GO spectra show different peaks in the range of 4000-600 cm^{-1} that is confirmation of GO formation, these peaks are due to different groups present on surface of GO [1, 2].

XRD technique mostly used for characterization of crystalline type materials from this we obtained information about d-spacing between the layers of material. Graphite XRD show peak (002) at $2\theta \sim 26.54$ with d spacing 3.33 A°, while the GO having new peak (001) at $2\theta \sim 10.37$ with d spacing 8.71 A°, Peak value shifting to lower 2θ with enhancing d-spacing is in the favour of GO confirmation, also peak intensity lower in GO as compared to graphite and peak broadening in GO as compared to graphite, as shown in figure 4.1.3 [3, 4].

TGA technique is used to check the thermal stability of materials,the graphite have only 5.3 % weight loss up to 700 °C due to removal of absorbed moisture of graphite powder. In GO having 11.5 % weight loss due to the interrupted water molecules on the surface of GO , 25.6 % weight loss up to 200 °C due to loss of less stable oxygen containing functional groups like epoxy and 47.3 % weight loss at 300 °C due to pyrolysis of most stable functional groups like carbonyl as shown in figure 4.1.4 [5, 6].

SEM analysis of Graphite and GO at different magnification like (100 µm, 50 µm, 10 µm, 5 µm and 0.5 µm) as shown in the figure 4.1.5, shows that graphite powder have layers firmly stacked and closed together while in GO layers are loosely stacked with disorder and corrugation, similarly in GO sheets looks like crumped having enhanced spacing between them [7] [8].

1,4-XDA linker molecule having peak at different region in FTIR spectrum, shown characteristic primary amine peaks at 3405 and 3361 cm^{-1} , similarly also shown the di-substituted benzene ring peak at 831 cm^{-1} as shown in the figure 4.16 and described in table 4.1.3 .

2,6-DAP linker molecule having peak at different region in FTIR spectrum, have characteristic primary amine peaks at 3345 and 3218 cm^{-1} as shown in the figure 4.1.7 and described in table 4.1.4 FOG-X-A framework having peak at different region in FTIR spectrum, have characteristic secondary amine peaks at 3329 cm^{-1} indication of attachment of

linker molecule with GO , C=O peak at 1621 cm^{-1} is also indication of framework formation as shown in the figure 4.1.8 and described in table 4.1.5 [9, 10].

FOG-X-B framework having peak at different region in FTIR spectrum, have characteristic peaks at 3440 and 3332 cm^{-1} these are due to either primary and secondary amine , in this framework some side have attached proper with GO to form secondary linkage and some side have no available groups for intercalation they remain as primary amine , it show also C=O peak at 1623 cm^{-1} as shown in the figure 4.1.9and described in table 4.1.6 [11].

FOG-X-C framework having peak at different region in FTIR spectrum, have no characteristic peaks in the region of primary and secondary amine , in this as the concentration of linker molecules increased reduced the GO, they show C=O peak at 1655 cm^{-1} and C-O epoxy at 982 cm^{-1} as shown in the figure 4.10 and described in table 4.1.7 [10].

FOG-D-A framework having peak at different region in FTIR spectrum, have characteristic secondary amine peaks at 3342 cm^{-1} is indication for proper linkage of linker molecule in GO layers , similarly shown C=O peak at 1605 cm^{-1} and benzene di-substituted peak at 831 cm^{-1} as shown in the figure 4.11 and described in table 4.1.8 [9].

FOG-D-B framework having peak at different region in FTIR spectrum, have no characteristic peaks in the region of above 3000 cm^{-1} so there is no primary nor secondary amine peak the linker molecule reduced the GO as shown in the figure 4.12 and described in table 4.1.9 [12].

FOG-D-C framework having peak at different region in FTIR spectrum, have no characteristic Primary and secondary amine peaks and it have reduced graphene type spectrum as shown in the figure 4.13 and described in table 4.1.10 [10, 12].

GO reacting with 1,4-XDA to form (FOG-X-A) framework having 2θ peak shifting to lower value at 7.17,having decreased intensity and also broadening of peak is evidence for formation of framework. Framework (FOG-X-B) have little peak at 2θ~ 7.86 having 145 intensity, similarly for framework (FOG-X-C) have little peak around 2θ~ 8.49, from all these the framework FOG-X-A is proper linkage of 1,4-XDA intercalation with GO [9, 13, 14].

GO reacting with 2,6-DAP to form (FOG-D-A) framework having 2θ peak shifting to lower value at 7.34 with decreased intensity and also broadening of peak is evidence for formation

of framework. Framework (FOG-D-B) have no peak in the range of 2θ ≤ 10, similarly for framework (FOG-X-C) have no peak in the range of 2θ ≤ 10, from all these the framework FOG-D-A is proper linkage of 2,6-DAP intercalation with GO [9, 13, 14].

SEM analysis of framework of FOG-X-A and FOG-D-A at different magnification like (0.5 µm, 5 nm and 1 nm) as shown in the figure 4.4.1, shows that FOG-X-A have wrinkled curved morphology having look like stacked separated layers and mesoporous type structure similarly in FOG-D-A look like layered by layered structure having separated layers, cross-linked type as shown in figure 4.13 [10, 15, 16] .

Thermal stability of framework FOG-X-A and FOG-D-A have been measured through thermal gravimetric analyzer, shows that FOG-X-A loss 24 % weight loss up to 100 °C due to absorbed moisture , 30 % weight loss up to 200 °C due to the removal of less stable molecules while 41 % weight loss up to 300 °C due to removal of more stable molecules in framework, similarly for FOG-D-A 12 % weight loss up to 100 °C due to loss of moisture and 51 % weight loss due to less stable molecules on the surface of framework while 57 % weight loss up to 200 °C due to removal of more stable groups, as compared to both FOG-X-A is more stable as compared to FOG-D-A [10, 17].

Surface area of sample was measured by Brunauer-Emmett-Teller instrument was measured at 77 K using N2 as an adsorption gas. The measured surface area of GO, FOG-X-A and FOG-D-A, surface area enhance from GO to linker due to more spacing between the layers of GO are given in table 4.5 [9, 16, 18].

In order to examine the performance of as-fabricated graphene materials for supercapacitor application, three electrode system was used using FOG X-A, FOG X-B, FOG X-C, FOG D-A, FOG D-B and FOG D-C as working electrode materials, respectively, with Ag/AgCl as a reference electrode and a platinum (Pt) as counter electrode. The measurements were carried out at the ambient temperature using 1 M H_2SO_4 aqueous electrolyte. Electrochemical tests such as cyclic voltammetry (CV), galvanostatic charge discharge and electrochemical impedance spectroscopy (EIS) were performed.

CV was done for all synthesized samples from 0.2 to 0.8 at different scan rates i-e 10 mVs^{-1}, 50 mVs^{-1} and 100mVs^{-1}. The curves indicate the oxidation and reduction behaviour of the samples used and the prominent faradic redox peaks can be observed in Figure. The peaks show the pseudocapacitive behaviour. FOG X-A exhibits the highest redox peaks at any scan

rate which is ascribed to the redox behaviour of the intercalated amine groups. By increasing the scan rate, the quasi-symmetric redox peaks and the analogous CV curve shapes are witnessed, proposing the ideal pseudocapacitive performance and the rate proficiencies or capabilities of the fabricated electrode materials[19, 20]. Furthermore, on increasing scan rate the cathodic peaks shifts towards the lower potential while the anodic peaks move to higher potential because of the insufficient of the ions from electrolyte too the graphene layers. At the same time, the cathodic current density decreases and increase in the anodic current density occurs which is the indicative of low resistance and rapid redox reaction at the electrode/electrolyte interface. The specific capacitance values are calculated by using formula shown in equation ()

The specific capacitance for all samples shown in table indicates that the sample FOG X-A has the highest $\mathbf{C_{sp}}$ value i-e 360Fg^{-1} at 20mVs^{-1} whereas the lowest value is observed for the FOG D-C i-e 29.37 Fg^{-1} at 20mVs^{-1}. The figure is the descriptive picture of the results indicates the maximum specific capacitance value for the FOG X-A

The galvanostatic charge–discharge is the complimentary technique to justify the above results. The charging discharging curves observed in Fig 4.12.2 (a),(b) for all the synthesized samples are non- symmetric[21]. This behaviour attributes to the pseudocapacitive nature of the materials. If we focus on the curves we can see that the small potential drop or IR drop is observed for the FOG X-A and the largest for the FOG D-C. IR drop is the sudden potential drop due to the internal electrode resistance, greater the potential drop lesser will be the efficiency of the electrode material and smaller will be the specific capacitance. This shows that FOG X-A is the best material for the supercapacitor with least potential drop.

Electrochemical impedance spectroscopy (EIS) was used to examine the charge transfer behaviour in GOF (graphene oxide frameworks) based electrodes. Fig.4.12.3 illustrates the Nyquist plot of fabricated modified graphene materials based electrodes, which we have recorded at 0.4V in the frequency range of 100 kHz to 0.01Hz. The Nyquist plot comprises of tiny semi-circular part in the high frequency region and almost vertical line in the low frequency region. As in high frequency region a semi-circular arc is observed in the plots of all samples which is associated with the electron transfer mechanism at the interface between the electrolyte and electrode. It is clear from the plot that FOG X-A shows smallest semi-circle in high frequency region while FOG D-C shows largest semi-circle at large frequency. So it is indicative of the small charge transfer resistance in case of earlier FOG X-A as

compared to the FOG D-C. The larger semicircle for FOG D-A suggests that it has a higher charge transfer resistance because of the restacking and aggregation in the reduction process. The straight line of the plot which is connected to the semicircular region shown in Fig. is the indicative of Warburg impedance (WI) that is the measure of the resistance to the diffusion of the electrolyte in the system [22, 23]. It is evident that incase of FOG X-A the slop is linear close to x-axis, the WI is minimum which means it facilitates the diffusion of electrolyte due to having increased spacing between the layers . Whereas, WI is maximum in case of FOG D-C due to very large linear part which reveals that it has large resistance to the electrolyte diffusion. These results support the higher specific capacitance value observed for the FOG X-A (table). This impedance study clearly demonstrates and validates the previous results in terms of charge kinetics.

However the carboxyl groups on the edges might react with 1,4-XDA or 2,6-DAP through amide linkage shown in (Scheme 2 and 3). FOG was synthesized through 'Reaction first then Reduction' process. 1,4-XDA or 2,6-DAP molecules were inserted into the space of graphene sheets and prevent them from restacking[23].

Zohaib

ORIGINALITY REPORT

%11	%2	%11	%3
SIMILARITY INDEX	INTERNET SOURCES	PUBLICATIONS	STUDENT PAPERS

PRIMARY SOURCES

1	Spyrou, Konstantinos, and Petra Rudolf. "An Introduction to Graphene", Functionalization of Graphene, 2014. Publication	%3
2	Xiangning Lu, Liyi Li, Bo Song, Kyoung-sik Moon, Ningning Hu, Guanglan Liao, Tielin Shi, Chingping Wong. "Mechanistic investigation of the graphene functionalization using p - phenylenediamine and its application for supercapacitors", Nano Energy, 2015 Publication	%3
3	Sekhar C. Ray. "Application and Uses of Graphene Oxide and Reduced Graphene Oxide", Elsevier BV, 2015 Publication	%1
4	Diseko Boikanyo, Monaheng L. Masheane, Lebea N. Nthunya, Shivani B. Mishra, Sabelo D. Mhlanga. "Carbon-supported photocatalysts for organic dye photodegradation", Elsevier BV, 2018 Publication	<%1

5	M. Sohail, M. Saleem, Sana Ullah, Noor Saeed, Ayesha Afridi, Majid Khan, M. Arif. "Modified and improved Hummer's synthesis of graphene oxide for capacitors applications", Modern Electronic Materials, 2017 Publication	<%1
6	dspace.lboro.ac.uk Internet Source	<%1
7	Submitted to University of St Andrews Student Paper	<%1
8	Wang, S.G.. "DNA biosensors based on self-assembled carbon nanotubes", Biochemical and Biophysical Research Communications, 20041224 Publication	<%1
9	Ming, Hai, Jun Ming, Shu Tian, Qun Zhou, Hui Huang, Yang-Kook Sun, Junwei Zheng, and Seung-Min Oh. "Surfactant-assisted synthesis of Fe2O3 nanoparticles and F-doped carbon modification toward an improved Fe3O4@CFx/LiNi0.5Mn1.5O4 battery", ACS Applied Materials & Interfaces Publication	<%1
10	Submitted to Indian Institute of Science, Bangalore Student Paper	<%1

11	C. Sasirekha, S. Arumugam. "Electrochemical performance of zinchydroxide Zn(OH)2 nanosheet for supercapacitor application", AIP Publishing, 2017 Publication	<%1
12	Bhanudas Naik, V.S. Prasad, Narendra Nath Ghosh. "A simple aqueous solution based chemical methodology for synthesis of Ag nanoparticles dispersed on mesoporous silicate matrix", Powder Technology, 2010 Publication	<%1
13	www.nature.com Internet Source	<%1
14	Submitted to The University of Manchester Student Paper	<%1
15	Goki Eda. "Chemically Derived Graphene Oxide: Towards Large-Area Thin-Film Electronics and Optoelectronics", Advanced Materials, 04/28/2010 Publication	<%1
16	d-nb.info Internet Source	<%1
17	www.faqs.org Internet Source	<%1
18	Xinming Chen, Stephen J. Romaniello, Achim	<%1

D. Herrmann, Laura E. Wasylenki, Ariel D. Anbar. "Uranium isotope fractionation during coprecipitation with aragonite and calcite", Geochimica et Cosmochimica Acta, 2016
Publication

19	O'Hayre, Ryan, Suk-Won Cha, Whitney Colella, and Fritz B. Prinz. "Chapter 7: Fuel Cell Characterization", Fuel Cell Fundamentals, 2016. Publication	<%1
20	Submitted to VIT University Student Paper	<%1
21	Submitted to Higher Education Commission Pakistan Student Paper	<%1
22	J. Xie, T. Tanaka, N. Imanishi, T. Matsumura, A. Hirano, Y. Takeda, O. Yamamoto. "Li-ion transport kinetics in LiMn2O4 thin films prepared by radio frequency magnetron sputtering", Journal of Power Sources, 2008 Publication	<%1
23	Jin, Lingling, Xiaowei Li, Hai Ming, Haohe Wang, Zhenyong Jia, Yu Fu, Jason Adkins, Qun Zhou, and Junwei Zheng. "Hydrothermal synthesis of Co3O4 with different morphologies towards efficient Li-ion storage", RSC Advances, 2014.	<%1

	Publication	
24	www.science.gov Internet Source	<%1
25	www.whxb.pku.edu.cn Internet Source	<%1
26	Songfeng Pei, Hui-Ming Cheng. "The reduction of graphene oxide", Carbon, 2012 Publication	<%1

EXCLUDE QUOTES	ON	EXCLUDE MATCHES	< 5 WORDS
EXCLUDE BIBLIOGRAPHY	ON		